energy&fuels

pubs.acs.org/EF

Article

Elucidating Biomass-Derived Pyrolytic Lignin Structures from Demethylation Reactions through Density Functional Theory Calculations

Raiza Manrique, Evan Terrell, Pavlo Kostetskyy, Farid Chejne, Mariefel Olarte, Linda Broadbelt, and Manuel García-Pérez*

Cite This: *Energy Fuels* 2023, 37, 5189−5205

Read Online

ACCESS | Metrics & More | Article Recommendations | Supporting Information

ABSTRACT: Pyrolytic lignin is a fraction of pyrolysis oil that contains a wide range of phenolic compounds that can be used as intermediates to produce fuels and chemicals. However, the characteristics of the raw lignin structure make it difficult to establish a pyrolysis mechanism and determine pyrolytic lignin structures. This study proposes dimer, trimer, and tetramer structures based on their relative thermodynamic stability for a hardwood lignin model in pyrolysis. Different configurations of oligomers were evaluated by varying the positions of the guaiacyl (G) and syringyl (S) units and the bonds βO4 and β5 in the hardwood model lignin through electronic structure calculations. The homolytic cleavage of βO4 bonds is assumed to occur and generate two free radical fragments. These can stabilize by taking hydrogen radicals that may be in solution during the intermediate liquid (pathway 1) formation before the thermal ejection. An alternative pathway (pathway 2) could occur when the radicals use intramolecular hydrogen, turning themselves into stable products. Subsequently, a demethylation reaction can take place, thus generating a methane molecule and new oligomeric lignin-derived molecules. The most probable resulting structures were studied. We used FTIR and NMR spectra of selected model compounds to evaluate our calculation approach. Thermophysical properties were calculated using group contribution methods. The results give insights into the lignin oligomer structures and how these molecules are formed. They also provide helpful information for the design of pyrolysis oil separation and upgrading equipment.

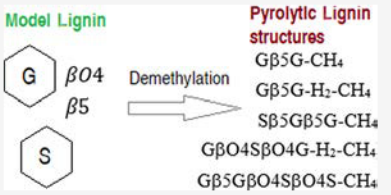

1. INTRODUCTION

Biomass pyrolysis is an extensively studied thermochemical process transforming raw biomass into fuels and chemicals.[1] Small lignocellulosic material particles (less than 2 mm) are subjected to rapid heating rates up to bed temperatures of 500 °C to produce vapors/gases and char. The vapors stay in the reactor for less than 2 s to avoid secondary reactions.[2] Pyrolysis oil comprises hundreds of chemical monomeric and oligomeric compounds and between 10 and 30 wt % of water.[3] The aromatic oligomers found in this heavy fraction, often called pyrolytic lignin, are an important bio-oil fraction[4] coming mainly from the depolymerization of lignin during the pyrolysis process at rapid heating rates and short hot vapor residence time (<1 s). These compounds are valuable platform chemicals that can contribute to the profitability of biomass pyrolysis with economic separations.

Lignin is a tridimensional aromatic polymer composed of three basic units: p-hydroxyphenyl (H), guaiacyl (G), and syringyl (S). The proportion of these units depends on the biomass species. Softwood lignin mainly comprises G units, hardwood lignin comprises a mixture of G and S units, and grass lignin contains three moieties.[5] The bonds of basic units can be divided into three types: ether bonds (βO4, αO4, γO4) are the most prevalent and represent 60−70% of the lignin bonds; carbon−carbon bonds (5-5, β5, β1), 30−40%, and ester bonds are few and exist mainly in herbaceous plants.[6] In addition, the methoxyl (O−CH_3) and phenolic hydroxyl (Ph-OH) groups in the aromatic rings are the two most important functional groups in lignin units.[7] All of these characteristics of the lignin polymer structure make it difficult to establish a pyrolysis mechanism and know the features of the pyrolytic lignin structure.

A chain reaction mechanism can explain lignin depolymerization during the pyrolysis process. An important study by Hosoya et al.[8] showed the char formation of various lignin compounds during this process using monophenols as model compounds. The products were identified through ion-gas chromatography−mass spectrometry and gas chromatography−mass spectrometry (GCMS). They proposed that the o-quinone methide—initiated from the H-abstraction of the phenolic hydroxyl groups—is an important intermediate for lignin char formation during pyrolysis. Jiang et al.[9] studied the

Received: December 30, 2022
Revised: February 25, 2023
Published: March 13, 2023

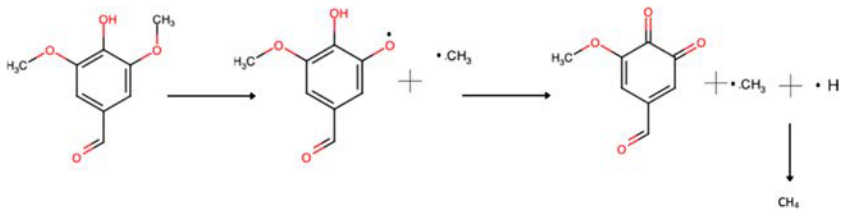

Figure 1. Demethylation mechanism reproduced with permission from ref 17. Copyright 2023 Elsevier.

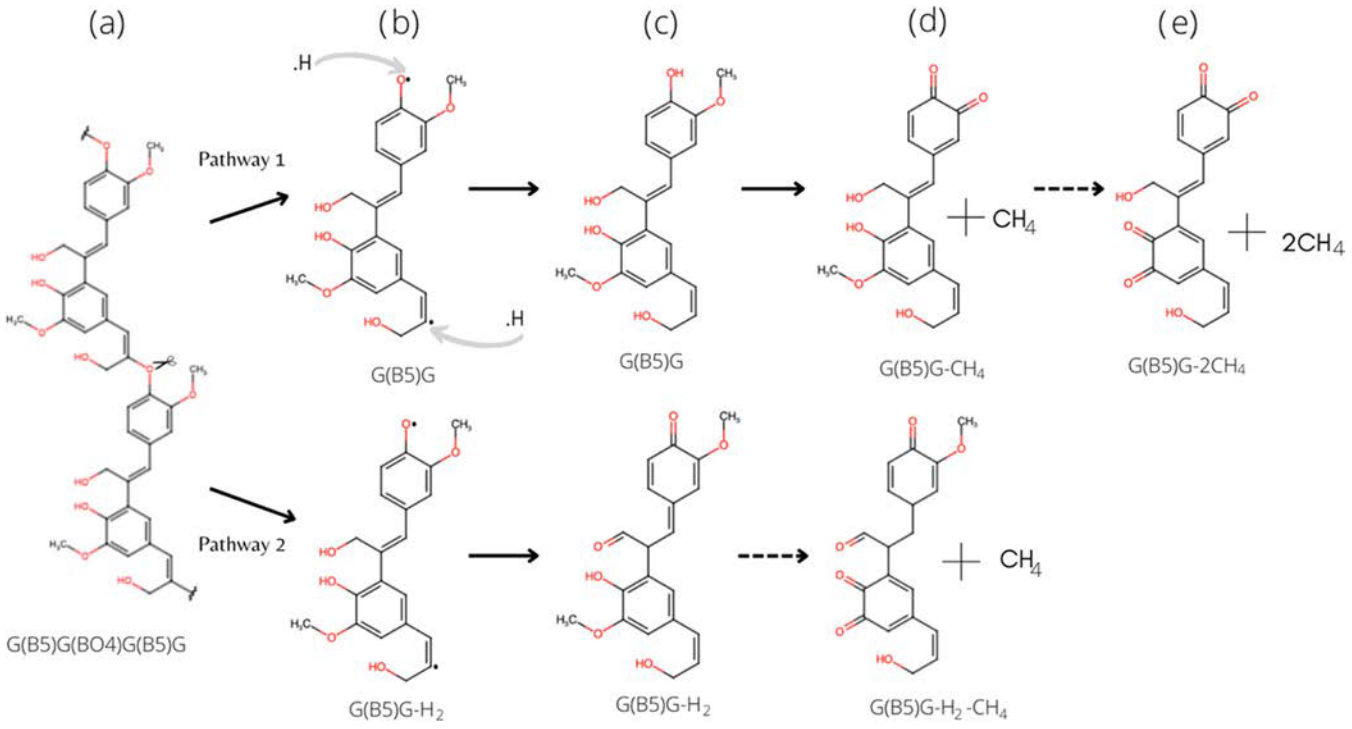

Figure 2. Proposed dimer decomposition mechanism. (a) Model lignin; (b) radical fragments; (c) balanced step; and (d and e) demethylation reaction.

model compound phenethyl phenyl ether (PPE), four other lignin-derived radicals, and two primary products (G and S units) to confirm possible interactions between lignin pyrolysis primary and secondary reactions using density functional theory (DFT) calculations and analytical experiments using a Py-GC/MS (pyrolysis gas chromatography−mass spectrometry). They used the homolysis radical mechanism and bond dissociation energies to estimate the interactions during the lignin pyrolysis process. The results indicate that the formed radicals can be stabilized by lignin and its derived pyrolytic products. The G and S units and the cellulose products act as hydrogen donors to form stable hydrogenated products. Later, Hu et al.[10] studied hydroxyl-assisted hydrogen transfer interaction in lignin pyrolysis through quantum mechanics calculations and pyrolysis experiments. They concluded that hydroxyl-assisted hydrogen could exist in the pyrolysis of lignin. Recent researchers have found that the methoxyl groups on GS-type products can quickly lose $-CH_3$ radicals via homolytic mechanisms and then through H-abstraction to form CH_4.[11−13] DFT calculations and analytical techniques suggest that lignin pyrolysis occurs through a homolysis radical mechanism.

In addition, Terrell et al.[14] studied raw lignin and pyrolysis lignin products with Fourier transform ion cyclotron resonance mass spectrometry (FT-ICR-MS) to propose a lignin fragmentation mechanism. They suggested potential trimer and tetramer structures based on the basic three units and four kinds of bonding between them, losing different functional groups. Fu et al.[15] studied the composition and structure of pyrolysis oligomers from different biomasses through electrospray ionization-mass spectrometry (EI-MS) and sequential mass spectrometry (MS^n). They classified pyrolysis bio-oil oligomers and concluded that lignin-derived oligomers are formed by dehydration, decarboxylation, and demethylation. This is consistent with lignin pyrolysis products, i.e., the formation of gas products, such as CO, CO_2, and CH_4,[16,17] which can be obtained via decarboxylation, decarbonylation, and demethylation, respectively.

To understand lignin pyrolysis mechanisms, it is important to study their properties, e.g., boiling point, the heat of vaporization, Hansen solubility parameters, standard enthalpy, and Gibbs free energy. Group contribution methods are widely used to estimate the thermophysical properties of pure compounds that may be very difficult to measure experimentally. This method consists of dividing the molecule into known small groups and calculating their properties to obtain those of the original molecule through addition rules. Fonts et al.[18] proposed a chemical composition of pyrolysis bio-oil obtained from biomass and determined its thermophysical properties through *ab initio* calculations and estimation

https://doi.org/10.1021/acs.energyfuels.2c04292
Energy Fuels 2023, 37, 5189−5205

Table 1. Initial Assignments of the Oligomers Studied through Pathways 1 and 2

dimers		trimers		tetramers	
pathway		pathway		pathway	
1	2	1	2	1	2
G(β5)G	G(β5)G-H_2	G(β5)G(βO4)S	G(β5)G(βO4)S-H_2	G(β5)G(βO4)S(βO4)S	G(β5)G(βO4)S(βO4)S-H_2
G(βO4)G	G(βO4)G-H_2	G(βO4)G(βO4)S	G(βO4)G(βO4)S-H_2	G(βO4)S(β5)G(βO4)S	G(βO4)S(β5)G(βO4)S-H_2
G(βO4)S	G(βO4)S-H_2	S(βO4)S(β5)G	S(βO4)S(β5)G-H_2	G(βO4)S(βO4)S(β5)G	G(βO4)S(βO4)S(β5)G-H_2
S(β5)G	S(β5)G-H_2	G(βO4)S(βO4)G	G(βO4)S(βO4)G-H_2	S(β5)G(β5)G(βO4)S	S(β5)G(β5)G(βO4)S-H_2
S(βO4)G	S(βO4)G-H_2	S(β5)G(β5)G	S(β5)G(β5)G-H_2	S(β5)G(βO4)G(βO4)S	S(β5)G(βO4)G(βO4)S-H_2
S(βO4)S	S(βO4)S-H_2	S(β5)G(βO4)G	S(β5)G(βO4)G-H_2	S(β5)G(βO4)S(β5)G	S(β5)G(βO4)S(β5)G-H_2
		S(βO4)G(β5)G	S(βO4)G(β5)G-H_2	S(β5)G(βO4)S(βO4)G	S(β5)G(βO4)S(βO4)G-H_2
		S(βO4)G(BO4)G	S(βO4)G(BO4)G-H_2	S(βO4)G(β5)G(βO4)S	S(βO4)G(β5)G(βO4)S-H_2
				S(βO4)G(βO4)S(β5)G	S(βO4)G(βO4)S(β5)G-H_2
				S(βO4)S(β5)G(β5)S	S(βO4)S(β5)G(β5)S-H_2
				S(βO4)S(β5)G(βO4)G	S(βO4)S(β5)G(βO4)G-H_2
				S(βO4)S(βO4)G(β5)G	S(βO4)S(βO4)G(β5)G-H_2

methods. High-molecular-mass (HMM) and low-molecular-mass (LMM) pyrolytic lignin were used to calculate the heavy fraction properties; however, the calculated critical temperature had a very low negative value, which is irregular. This inconsistency could be due to difficulty in selecting the property's calculation method. This study recommends isolating some oligomers to determine the thermophysical properties experimentally. Terrell[19] estimated the Hansen solubility parameters for biomass conversion products using an adaptable group contribution method. The solubility parameter was calculated for 35 lignin-derived oligomers.

This manuscript aims to evaluate different lignin oligomer structure representations from fast pyrolysis based on their relative stabilities estimated by electronic structure calculations. Oligomers' physicochemical properties are calculated by applying the group contribution method.

2. METHODOLOGY

2.1. Assignment of Pyrolytic Lignin Oligomers. A model hardwood lignin was used to evaluate the assignment of pyrolytic lignin oligomers. In this manuscript, we studied the most probable demethylation mechanism (see Figure 1). The demethylation reaction pathway of the oligomer lignin structure was applied to model oligomers, and the reaction pathways were produced by three-step reactions. First, the ether bond O−CH_3 ruptures to form a free radical and methyl; this homolytic cleavage absorbs energy. Then, the intermediate radical undergoes dehydrogenation to form the quinone product. Finally, hydrogen and methyl bond to form methane.[17] First and sequential demethylations (up to 3) of these assignments were completed at a gas phase, a typical fast pyrolysis temperature of 773.15 K, and a pressure of 101 325 Pa. Homolysis of the O−CH_3 bond can occur after fragment stabilization by increasing the temperature to 450 °C approx.[20]

A chain reaction mechanism can explain pyrolytic lignin depolymerization.[20,21] Figure 2 shows the proposed mechanism of the first assignment of dimers presented in Table 1. Under pyrolysis conditions (rapid heating up to 500 °C and inert atmosphere), a model lignin composed of S and G units bonds with βO4 and β5-G(β5)G(βO4)G(β5)G-, depolymerizes through βO4, and breaks the bonds between its dimer units (Figure 2a). This bond is one of the weakest and can be thermally cleaved at 200−250 °C. Therefore, the chain mechanism is primarily initiated by direct βO4 homolysis of the model lignin to generate two or more free radical fragments,[22,23] i.e., dimers, trimers, or tetramers. Figures S1 and S2 show the mechanism when the radical fragments are trimers and tetramers, respectively. The radicals are in the oxygen and carbon where the βO4 bond was located, as shown in Figure 2b. These radical fragments can stabilize by taking hydrogen radicals that may be in solution during the formation of the intermediate liquid before thermal ejection[24] (pathway 1). In this way, the hydrogen lost due to the homolytic rupture is recovered, and the structure in this case is G(β5)G. An alternative pathway could occur when the radicals use intramolecular hydrogen and turn themselves into stable products (pathway 2). The assignment of this pathway is named (G(β5)G-H_2) because the structure loses two hydrogens due to the homolytic rupture. Both pathways are shown in detail in Figure 2c. The above are the initial structures we propose to evaluate the demethylated structures of pyrolytic lignin at subsequent stages of the pyrolysis process. Table 1 presents all initial assignments for the dimer, trimer, and tetramer for both pathways. Then, homolysis of the O−CH_3 bond can occur by increasing the temperature to 450 °C approx.[20] Figure 2 shows the proposed mechanism of the first assignment of dimers presented in Table 1. Figures S1 and S2 show the mechanism when the radical fragments are trimers and tetramers, respectively.

Letters G and S represent its syringyl and guaiacyl monomers, respectively. Linkages βO4 and β5 connect two monomers. These bonds are evaluated at different configurations because they are the most relevant in the lignin structure. Recent studies by Fan et al.[25] and Lei et al.[26] have shown free radicals *in situ* and mentioned a pathway that can originate from the βO4 bond cleavage and be transformed into a quinone structure. The scission of the βO4 bond is generally the initial step for the model lignin decomposition. As a result of this reaction, radical fragments are generated, which can be stabilized by hydrogen molecules, as suggested elsewhere.[9] After this balanced step, the demethylation reaction could occur with the increase in temperature. Table 1 shows the assignments based on the permutations of two monomer units and two bonds to single, double, and triple demethylation in the pyrolitic lignin structures through two different pathways. They differ in the way they stabilize the radical fragments of the model hardwood lignin after the homolytic cleavage in the first stage of pyrolysis (discussed in detail in the next section). The assignments were based on the lignin oligomers proposed elsewhere.[14]

https://doi.org/10.1021/acs.energyfuels.2c04292
Energy Fuels 2023, 37, 5189−5205

The data set comprises 16 dimer, 98 trimer, and 46 tetramer structures for pathway 1 because the different positions in which the methoxy groups could be in the molecule were evaluated by assignment. The data set in the second pathway comprises 6 dimers, 8 trimers, and 12 tetramers because only the most stable structures per assignment in the first pathway were used to evaluate the structures. All structures were evaluated based on their relative thermodynamic stability through electronic structure calculations. The link between any unit and an S unit through β5 bonding was not considered because the S unit has two methoxy groups in the 3 and 5 carbon (these spaces are unavailable), according to Figure 1b.

2.2. DFT Computational Details. *2.2.1. Most Thermodynamically Stable Products.* Geometry optimization and frequency calculations of all reagents, intermediates, and products were performed using DFT with the Gaussian 16 program suite at M06-2X functional and the 6-311++G(d,p) basis set for the O, C, and H atoms.[27] Each equilibrium geometry for all calculations was verified to have no imaginary frequency. The most thermodynamically stable product structure was then assessed based on the reaction that yields the lowest Gibbs free energy change, i.e., this reaction is the most favorable structure. It should be noted that only close-shell calculations were performed to assess the stability of the demethylation products (oligomer-CH_3 or oligomer-H_2-CH_3), and the stabilities of the radical intermediates in the proposed mechanism were not assessed.

2.2.2. Estimation of FTIR and NMR Spectra of Most Stable Molecules. Once the thermodynamically stable molecule was identified, the Fourier transform infrared spectroscopy (FTIR) spectra were obtained. The frequency scale factor of the functional and basis set was 0.9567, according to the available literature.[28] Later, we calculated the theoretical proton nuclear magnetic resonance (^{1}H NMR) and carbon-13 nuclear magnetic resonance (^{13}C NMR) spectra using the gauge-independent atomic orbital (GIAO) method. It is necessary to understand the NMR since spectra strongly depend on the molecule structure because they are constantly in motion. Thus, we make sure to use the lowest energy structure of the molecule of interest. Vibrational frequencies calculated at the M06-2X functional and 6-311++G(d,p) level of theory were used to generate the FTIR and NMR spectra of the stable products. Also, NMR spectra of the typically used reference molecule—tetramethylsilane (TMS)—were calculated, and the shielding value was subtracted from the stable product spectrum to obtain the relative shifts. Generating information on the FTIR and NMR spectra of the new oligomeric molecules is of great practical importance because many of them are not available commercially. Thus, the calculated spectral information will help in assigning structures once appropriate bio-oil separation strategies have been implemented and experimental spectra of these molecules are obtained. Theoretical results may slightly differ among types of functional and basis sets and the type of reference molecule employed in FTIR and NMR estimations.

2.2.3. Estimation of FTIR and NMR Spectra of Model Compounds. Our calculation method was validated by comparing the estimated FTIR and NMR spectra with known phenolic molecules (vanillin, hydroquinone, and benzoquinone) with qualitative agreement observed for a number of peaks. The DMSO-d_6 solvent was used as a reference molecule in the simulated NMR spectra of model compounds to match the experimental results. The calculated spectra of oligomers were compared with those of pyrolytic lignin as another strategy to evaluate the validity of our FTIR estimations. The latter was obtained by cold-water precipitation and dichloromethane (DCM) extraction from commercial bio-oil (BTG, The Netherlands). The bio-oil is made from pine wood at 500 °C. The NMR results for model compounds were scaled to be plotted and compared with the experimental results using a factor of 50 000 and 200 000 for vanillin, 30 000 and 200 000 for hydroquinone, and 80 000 and 300 000 for benzoquinone for proton and carbon-13 NMR.

FTIR spectra were obtained using a Shimadzu IRPrestige 21 spectrometer equipped with a MIRacle single reflection ATR Ge probe. A drop of oil was applied to cover the crystal window, and the spectra were determined with 64 scans—600 to 4000 cm^{-1}—with a resolution of 4 cm^{-1}. The spectra were baseline corrected and band fitted between 1490 and 1850 cm^{-1} using 9 Gaussian bands according to ref 29. The results were scaled to be plotted and compared with the simulated results using a factor of 10 000 for vanillin, hydroquinone, benzoquinone, and pyrolitic lignin.

The ^{1}H NMR and ^{13}C NMR spectra were determined on a Bruker 500 Neo spectrometer equipped with a 5 mm Prodigy broadband cryoprobe with *Z*-axis gradients. Model compound (30 mg each) proton spectra were obtained at 500.13 MHz in DMSO-d_6 (0.6 mL), 30 °C with 16 scans, 90° pulse (12 μs), 3 s relaxation delay, and acquisition time of 4.4 s, 32 768 points, and a spectral width of 7463 Hz. Proton data were apodized with 1.3 Hz of line broadening. ^{13}C NMR spectra were acquired at 125.77 MHz with 90° pulse angle (10.0 μs), 1.08 s acquisition time, 2 s relaxation delay d1, and inverse-gated ^{1}H composite pulse decoupling using 4000 scans, a spectral width of 30 120.5 Hz, and 32 768 points. The FID was apodized with 8 Hz exponential line broadening of the model compounds.

2.3. Group Contribution to Estimate Thermophysical Properties. Group contribution methods for thermophysical property estimation rest on the assumption that forces between atoms in the same or different molecules have short ranges. Quantitative property−property relationships (QPPR) and quantitative structure−property relationships (QSPR) were applied to estimate the relevant thermophysical properties of the compounds. The parameters estimated in this study are the physical change, ideal gas, and condensed gas properties. For the physical change properties, normal boiling point (Stein and Brow method,[30] Satou et al. method,[31] and Yuan et al. method[32]), critical temperature (Lydersen method[33] and Joback method[34]), critical volume (Lydersen method[33] and Joback method[34]), critical pressure (Lydersen method[33]), and enthalpy of vaporization temperature (Joback and Reid[35] and QPPR methods) were estimated. The Hansen solubility parameters were calculated using the Stefanis & Panayiotou method.[36] The condensed gas properties consist of liquid heat capacity, which was calculated using the Chueh & Swanson method,[37] and solid heat capacity (Hurst and Harrison method[38]). Finally, the Harrison and Seaton method[39] was also employed to determine gas heat capacity. The ideal gas properties included gas heat capacity, standard Gibbs free energy, change in enthalpy, and change in entropy; they were calculated using electronic structure calculations. Complete equations and procedures are described elsewhere (Fonts et al.[40] 2021). Briefly, the functional groups of the different elements comprising the molecule were identified, and their numbers of frequency were summed up and then multiplied by

https://doi.org/10.1021/acs.energyfuels.2c04292
Energy Fuels 2023, 37, 5189−5205

Table 2. Most Thermodynamically Stable Structures of Demethylated Lignin Dimers

structure	label	molecular formula	molecular weight (amu)	ΔG_{rx} (kJ/mol)	ΔH_{rxn} (kJ/mol)	ΔS_{rxn} (J/mol-K)
			Pathway 1			
Gβ5G-CH_4	D1	$C_{19}H_{18}O_6$	342.84	−29.51	86.59	150.16
GβO4G-CH_4	D2	$C_{19}H_{18}O_6$	342.84	−10.77	108.02	153.66
GβO4S-CH_4	D3	$C_{20}H_{20}O_7$	372.69	−6.21	107.11	146.56
Sβ5G-CH_4	D4	$C_{20}H_{20}O_7$	372.69	−21.92	82.35	143.32
SβO4S-CH_4	D5	$C_{21}H_{22}O_8$	342.84	−27.14	86.32	146.75
SβO4G-CH_4	D6	$C_{20}H_{20}O_7$	372.12	−23.67	90.67	147.89
Gβ5G-$2CH_4$	D7	$C_{18}H_{14}O_6$	326.69	−44.63	176.13	285.52
			Pathway 2			
Gβ5G-H_2-CH_4	D1*	$C_{19}H_{16}O_6$	340.01	−4.77	116.83	157.29
GβO4G-H_2-CH_4	D2*	$C_{20}H_{20}O_6$	356.13			
GβO4S-H_2-CH_4	D3*	$C_{21}H_{22}O_7$	386.14			
Sβ5G-H_2-CH_4	D4*	$C_{20}H_{18}O_7$	370.10	0.74	116.13	149.25
SβO4S-H_2-CH_4	D5*	$C_{22}H_{24}O_8$	416.15			
SβO4G-H_2-CH_4	D6*	$C_{21}H_{22}O_7$	386.14			

their group contribution. The information collected is very important for engineering calculations.

3. RESULTS AND DISCUSSION

3.1. Simulated Structures. This study focused on the evaluation of pyrolytic lignin structures after demethylation reaction, as it is assumed to be one of the primary reactions that could occur after depolymerization.[41] Some studies also mentioned methane as one of the main gaseous products during lignin pyrolysis.[42,43] Homolysis of the O−CH_3 bond occurs at temperatures above 400 °C, the radical induces a rearrangement by substitution, and methylated aromatics are produced from subsequent reactions.[17,44] Additionally, the released methyl group reacts with hydrogen at the phenol position and forms methane (see Figure 2d), and the resulting structures following pathways 1 and 2 are G(β5)G-CH_4 and (G(β5)G-H_2-CH_4), respectively. Demethylation through pathway 2 cannot be given in all evaluated structures because a phenol group was used to stabilize the molecule in the last step. This reduces the availability of groups to form methane (dotted line). Finally, different types of demethylations can occur through pathway 1 (see Figure 2e). These possibilities were also simulated when performed once, twice, and thrice depending on the type of oligomer configuration. Hence, more than one demethylation can occur (dotted line) depending on the O−CH_3 available in the molecule for pathway 1. The formation of G(β5)G-$2CH_4$ (double demethylation) through pathway 1 could happen since O−CH_3 groups are available. Double and triple demethylations can be found in trimer and tetramer mechanisms.

The methylated aromatic oligomer structures become quinone products according to the mechanism used in this study, as shown in Figure 1c. They were specifically benzoquinones, which can be an intermediate compound or a final product in lignin thermal decomposition in the biomass pyrolysis process, as suggested in earlier work.[45,46] These types of compounds have been found to be intermediate products during biomass pyrolysis.[47,48] This mechanism is also proposed for trimers and tetramers, and their difference lies in the methoxy groups available for demethylation reactions once the molecule is balanced. The mechanism of trimers and tetramers can be observed in Figures S1 and S2 of the supplementary material.

3.1.1. Dimers. Table 2 shows the most thermodynamically stable dimer products per assignment of both pathways (those with lower Gibbs free energies out of the simulated molecules). The most probable oligomers in pathway 1 (see Figure 2) are structures D1 (Gβ5G-CH_4), D5 (SβO4S-CH_4), and D7 (D-Gβ5G-$2CH_4$). They have a β5 bond and are conjugated, containing alternating double bonds that allow overlapping between the adjacent π bonds. The selected dimers (Sβ5G) have S and G units connected by a β5 bond; thus, the stable structures have a conjugated C−C double bond. The molecular formulas of the proposed dimers present some differences in hydrogen loss related to methanol formation. These molecular formulas for oligomers are consistent with results obtained in previously reported work.[14] The dimers' Gibbs free energies are −29.5 and −44.6 kJ/mol for single and double demethylation, respectively. Kotake et al.[49] reported that the formation of the quinone methides could be attributed to the reduction of the stability of G units caused by the conjugated C−C double bond.

In the case of pathway 2, the initial radical structures were balanced using its intramolecular hydrogen. In this pathway, quinones are formed by the location of the radical in the upper part of the structure, and the other radical is balanced with the double bond in the aliphatic chain of the first unit. After that, the structures react to form methane and quinones through demethylation. However, in the evaluated structures, only D1* (Gβ5G-H_2-CH_4) and D4* (Sβ5G-H_2-CH_4) could continue the reactions (see Figure 2) because they contain the G units, which indicates the available methoxy and OH groups in the ring of the basic lignin unit, unlike the other structures balanced through pathway 2. The Gibbs free energy values were −4.77 and 0.74 KJ/mol, respectively. The molecules with unreported values indicate that after the chemical balance, those structures could not continue subsequent reactions due to the lack of OH and O−CH_3 groups (a representation of these structures can be seen in Table S1). D1* (Gβ5G-H_2-CH_4) is the most stable structure, probably because it is a conjugated one, as it occurs in the first pathway. Additionally, when the structures take the first route, it is possible that a second demethylation takes place due to the availability of methoxy and OH groups. On the contrary, in the second pathway balancing process, the structures lose that availability by forming quinones during stabilization. A detailed

https://doi.org/10.1021/acs.energyfuels.2c04292
Energy Fuels 2023, 37, 5189−5205

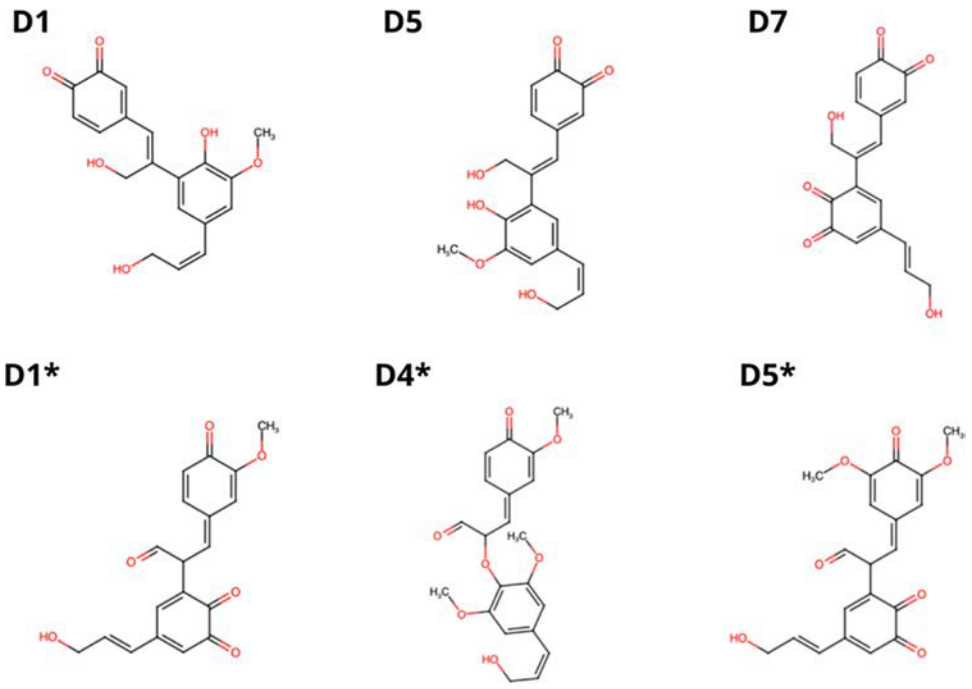

Figure 3. Detailed representation of the most stable dimers.

Table 3. Most Thermodynamically Stable Structures of Demethylated Lignin Trimers

structure	label	molecular formula	molecular weight (amu)	ΔG_{rxn} (kJ/mol)	ΔH_{rxn} (kJ/mol)	ΔS_{rxn} (J/mol-K)
			Pathway 1			
SβO4Gβ5G-CH_4	T1	$C_{30}H_{30}O_{10}$	550.55	−26.69	87.21	147.31
GβO4Sβ5G-CH_4	T2	$C_{30}H_{30}O_{10}$	550.55	−35.72	79.63	149.20
Gβ5GβO4S-CH_4	T3	$C_{30}H_{30}O_{10}$	550.55	−38.21	60.89	128.17
Sβ5GβO4G-CH_4	T4	$C_{30}H_{30}O_{10}$	550.55	−25.83	115.83	147.69
SβO4GβO4G-CH_4	T5	$C_{30}H_{30}O_{10}$	550.55	−31.74	87.47	154.18
Sβ5Gβ5G-CH_4	T6	$C_{30}H_{30}O_{10}$	550.55	−53.35	5.71	178.26
GβO4SβO4G-CH_4	T7	$C_{30}H_{30}O_{10}$	550.55	−45.67	107.36	147.98
GβO4GβO4S-CH_4	T8	$C_{30}H_{30}O_{10}$	550.55	−33.71	76.39	142.40
Sβ5Gβ5G-2CH_4	T9	$C_{29}H_{26}O_{10}$	534.51	−66.37	114.67	344.41
Sβ5Gβ5G-3CH_4	T10	$C_{28}H_{22}O_{10}$	518.47	−119.96	325.93	465.03
			Pathway 2			
SβO4Gβ5G-H_2-CH_4	T1*	$C_{30}H_{28}O_{10}$	548.16	13.51	96.16	141.85
GβO4Sβ5G-H_2-CH_4	T2*	$C_{30}H_{28}O_{10}$	548.16	12.95	107.82	156.21
Gβ5GβO4S-H_2-CH_4	T3*	$C_{30}H_{28}O_{10}$	548.16	11.29	106.81	152.77
Sβ5GβO4G-H_2-CH_4	T4*	$C_{30}H_{28}O_{10}$	548.16	30.67	78.86	141.68
SβO4GβO4G-H_2-CH_4	T5*	$C_{31}H_{32}O_{10}$	564.20			
Sβ5Gβ5G-H_2-CH_4	T6*	$C_{30}H_{28}O_{10}$	548.16	15.33	106.75	157.9
GβO4SβO4G-H_2-CH_4	T7*	$C_{31}H_{32}O_{10}$	564.20			
GβO4GβO4S-H_2-CH_4	T8*	$C_{31}H_{32}O_9$	548.20			

representation of the most stable dimers through pathways 1 and 2 is shown in Figure 3.

3.1.2. Trimers. Table 3 shows the information of the molecular formula and weight, Gibbs free energy, enthalpy, and entropy of the most stable trimers per assignment. Those that take pathway 1 (see Figure S1) are structures T6 (Sβ5Gβ5G-CH_4), T9 (Sβ5Gβ5G-2CH_4), and T10 (Sβ5Gβ5G-3CH_4) with Gibbs free energies of −53.3, −66.4, and −119.9 kJ/mol for single, double, and triple demethylation, respectively. These trimers are isomers (Sβ5Gβ5G) and have one S and two G units linked by two β5 bonds. The molecular formulas of the proposed trimers are $C_{30}H_{30}O_{10}$, $C_{29}H_{26}O_{10}$, and $C_{28}H_{22}O_{10}$, and their difference lies in the hydrogen loss related to methanol formation more than once. These molecular formulas are similar to the structures proposed by Terrell et al.[50] for lignin oligomers.

Trimers in pathway 2 have more structures after balancing, and it is possible that demethylation may occur if compared to the dimers due to the additional monomer providing available methoxy and OH groups depending on the assignment of the structure. In this route, trimers are balanced by their own atoms, thus producing quinones in the depolymerization stage of the pyrolysis process before the demethylation reaction; hence, a double quinone can be found in this oligomer structure (see Figure S1). Some of these balanced trimers can go through demethylation reactions due to the availability of

https://doi.org/10.1021/acs.energyfuels.2c04292
Energy Fuels 2023, 37, 5189−5205

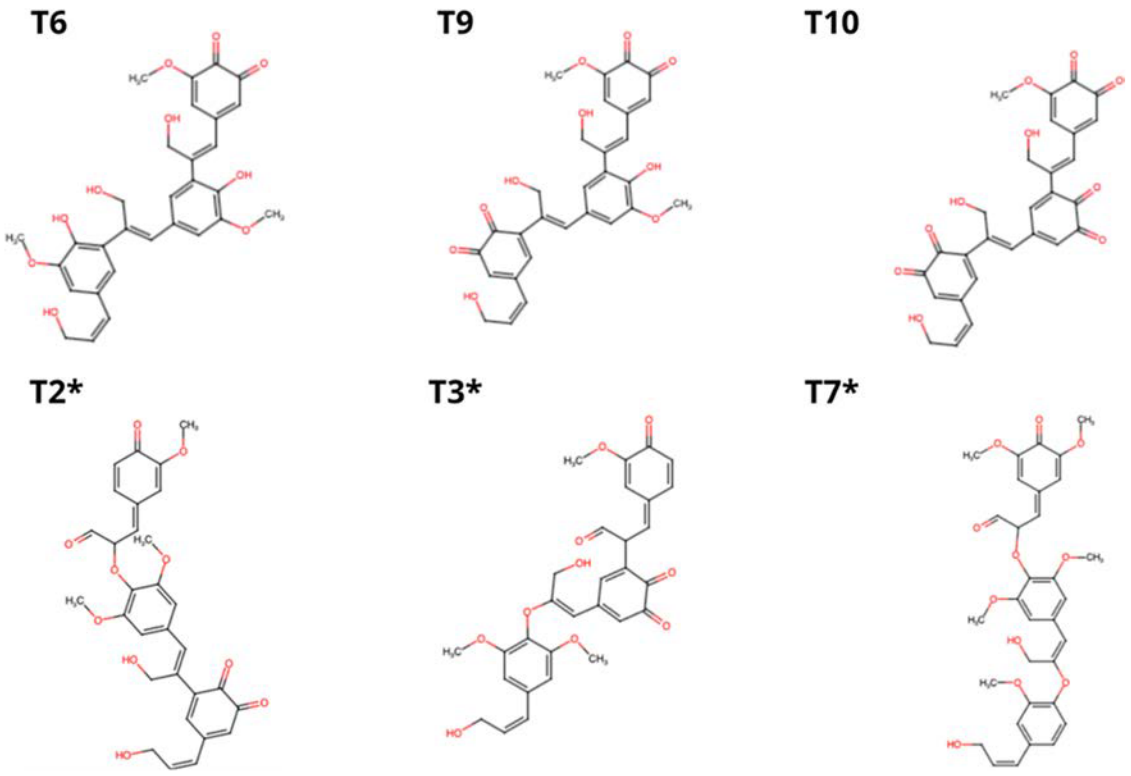

Figure 4. Detailed representation of the most stable trimers.

Table 4. Most Thermodynamically Stable Structures of Demethylated Lignin Tetramers

structure	label	molecular formula	molecular weight (amu)	ΔG_{rxn} (kJ/mol)	ΔH_{rxn} (kJ/mol)	ΔS_{rxn} (J/mol-K)
			Pathway 1			
GβO4Sβ5GβO4S-CH_4	OG1	$C_{41}H_{42}O_{14}$	758.26	−10.26	101.37	144.38
GβO4SβO4Sβ5G-CH_4	OG2	$C_{41}H_{42}O_{14}$	758.26	−29.16	78.67	144.38
Sβ5Gβ5GβO4S-CH_4	OG3	$C_{41}H_{42}O_{14}$	758.26	−24.93	84.47	145.38
Sβ5GβO4GβO4S-CH_4	OG4	$C_{41}H_{42}O_{14}$	758.26	−17.80	102.63	155.77
Sβ5GβO4Sβ5G-CH_4	OG5	$C_{41}H_{42}O_{14}$	758.26	−25.36	94.01	154.41
Sβ5GβO4SβO4G-CH_4	OG6	$C_{41}H_{42}O_{14}$	758.26	−30.14	92.69	158.86
SβO4Gβ5βO4S-CH_4	OG7	$C_{41}H_{42}O_{14}$	758.26	−29.19	82.13	143.99
SβO4GβO4Sβ5G-CH_4	OG8	$C_{41}H_{42}O_{14}$	758.26	−15.50	96.24	144.53
SβO4Sβ5Gβ5G-CH_4	OG9	$C_{41}H_{42}O_{14}$	758.26	−23.00	21.69	147.16
SβO4Sβ5GβO4G-CH_4	OG10	$C_{41}H_{42}O_{14}$	758.26	−29.72	52.78	154.29
SβO4SβO4Gβ5G-CH_4	OG11	$C_{41}H_{42}O_{14}$	758.26	−18.78	99.71	153.25
Gβ5GβO4SβO4S-CH_4	OG12	$C_{41}H_{42}O_{14}$	758.26	−31.00	87.47	149.89
GβO4SβO4Sβ5G-2CH_4	OG13	$C_{40}H_{38}O_{14}$	742.22	−49.37	42.10	291.70
Sβ5Gβ5GβO4S-3CH_4	OG14	$C_{39}H_{34}O_{14}$	726.19	−52.81	76.48	482.24
			Pathway 2			
GβO4Sβ5GβO4S-H_2-CH_4	OG1*	$C_{41}H_{40}O_{14}$	756.24	24.85	101.43	163.35
GβO4SβO4Sβ5G-H_2-CH_4	OG2*	$C_{41}H_{40}O_{14}$	756.24	21.52	97.63	154.12
Sβ5Gβ5GβO4S-H_2-CH_4	OG3*	$C_{41}H_{40}O_{14}$	756.24	17.36	100.54	152.50
Sβ5GβO4GβO4S-H_2-CH_4	OG4*	$C_{41}H_{40}O_{14}$	756.24	17.92	100.32	152.94
Sβ5GβO4Sβ5G-H_2-CH_4	OG5*	$C_{41}H_{40}O_{14}$	756.24	16.39	102.32	153.54
Sβ5GβO4SβO4G-H_2-CH_4	OG6*	$C_{41}H_{40}O_{14}$	756.24	16.96	105.58	158.51
SβO4Gβ5GβO4S-H_2-CH_4	OG7*	$C_{41}H_{40}O_{14}$	756.24	24.64	101.37	162.98
SβO4GβO4Sβ5G-H_2-CH_4	OG8*	$C_{41}H_{40}O_{14}$	756.24	11.75	101.71	146.77
SβO4Sβ5Gβ5G-H_2-CH_4	OG9*	$C_{41}H_{40}O_{14}$	756.24	13.12	102.87	150.03
SβO4Sβ5GβO4G-H_2-CH_4	OG10*	$C_{41}H_{40}O_{14}$	756.24	12.35	100.07	145.42
SβO4SβO4Gβ5G-H_2-CH_4	OG11*	$C_{41}H_{40}O_{14}$	756.24	19.08	99.87	153.86
Gβ5GβO4SβO4S-H_2-CH_4	OG12*	$C_{41}H_{40}O_{14}$	756.24	20.20	102.44	158.63

methoxy and OH groups in the molecule (the structures can be seen in Table S2). For this reason, trimers T5* (SβO4GβO4G-H_2-CH_4), T7* (GβO4SβO4G-H_2-CH_4), and T8* (GβO4GβO4S-H_2-CH_4) do not have the energy,

https://doi.org/10.1021/acs.energyfuels.2c04292
Energy Fuels 2023, 37, 5189−5205

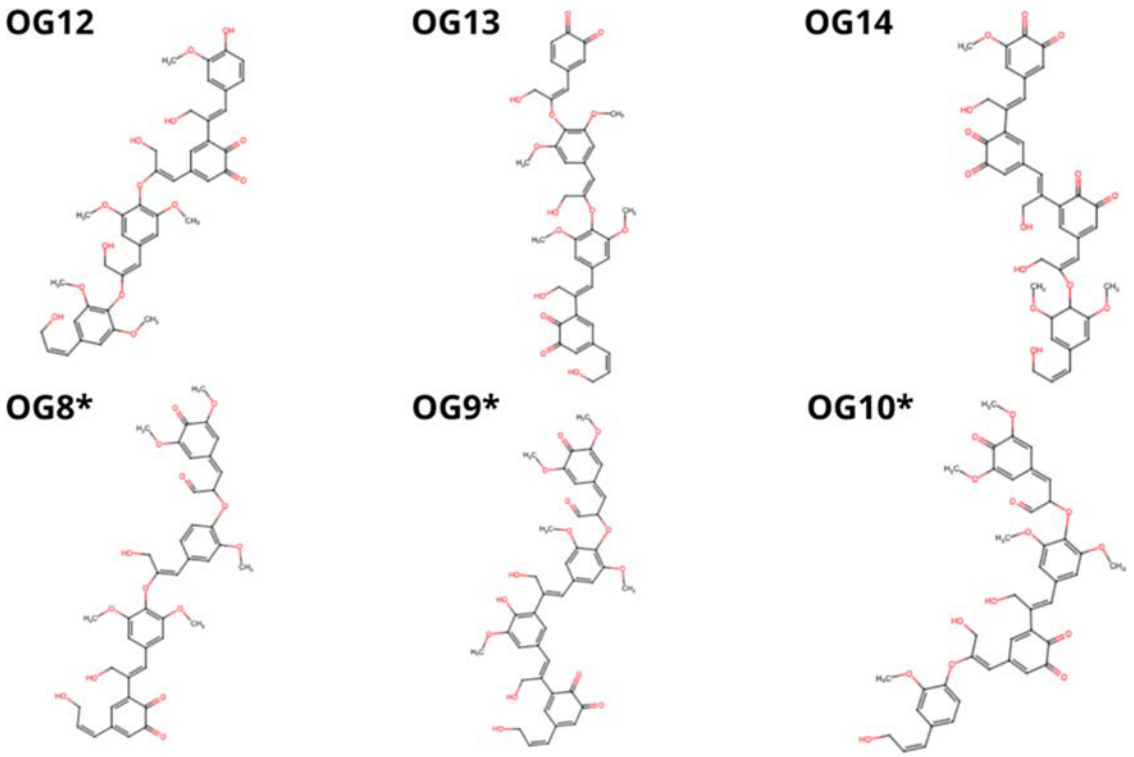

Figure 5. Detailed representation of the most stable tetramers.

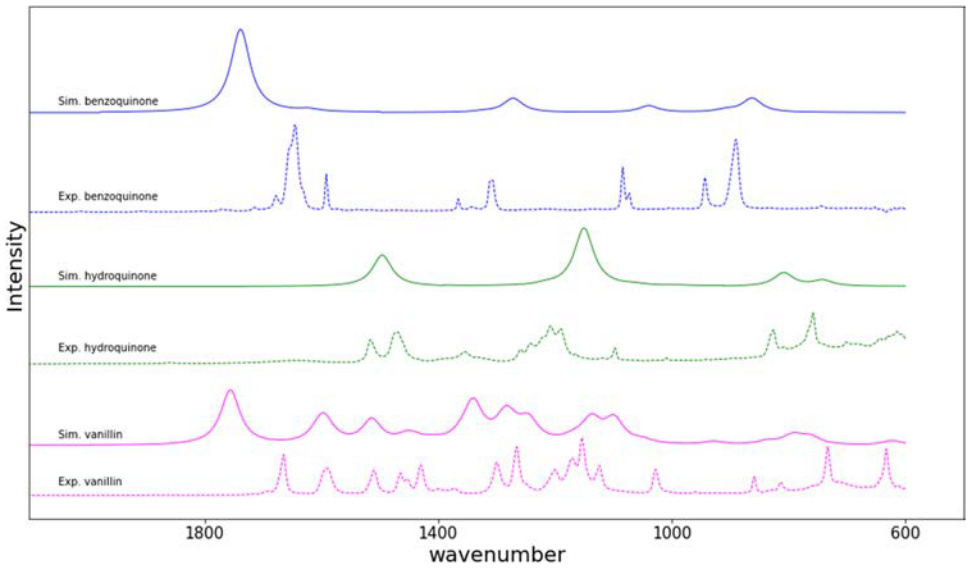

Figure 6. Fingerprint region of the FTIR spectra of model lignin compounds.

enthalpy, and entropy properties of reaction. Although the reaction energies are positive in these structures, the most probable trimers are T2* (GβO4Sβ5G-H_2-CH_4) and T3* (Gβ5GβO4S-H_2-CH_4) because they have values of 11.3 and 12.9 kJ/mol. Figure 4 shows a detailed representation of the most stable structure and T7* (GβO4SβO4G-H_2-CH_4) as an example of the trimer structure that could not undergo the demethylation reactions.

3.1.3. Tetramers. Table 4 shows the values of the thermodynamic properties of the most stable tetramers per assignment according to the proposed trimer mechanism in Figure S2. The ones that take pathway 1 are structures OG12 (Gβ5GβO4SβO4S-CH_4), OG13 (GβO4SβO4Sβ5G-$2CH_4$), and OG14 (Sβ5Gβ5GβO4S-$3CH_4$) with Gibbs free energies of −31.0, −49.4, and −52.8 kJ/mol for single, double, and triple demethylation, respectively. These oligomers have four monomeric units and, therefore, a greater possibility of subsequent demethylation reactions. For this reason, tetramers that have undergone more than one demethylation reaction are observed. The most probable tetramer structure for single demethylation is the assignment Gβ5GβO4SβO4S; it has two G and two S units linked by one β5 and βO4 bonds. Again, the β5 bonds are relevant in these oligomers because they facilitate the conjugate effect in this type of molecule.

In pathway 2, the most stable structures are OG8* (SβO4GβO4Sβ5G-H_2-CH_4), OG9* (SβO4Sβ5Gβ5G-H_2-

https://doi.org/10.1021/acs.energyfuels.2c04292
Energy Fuels 2023, 37, 5189−5205

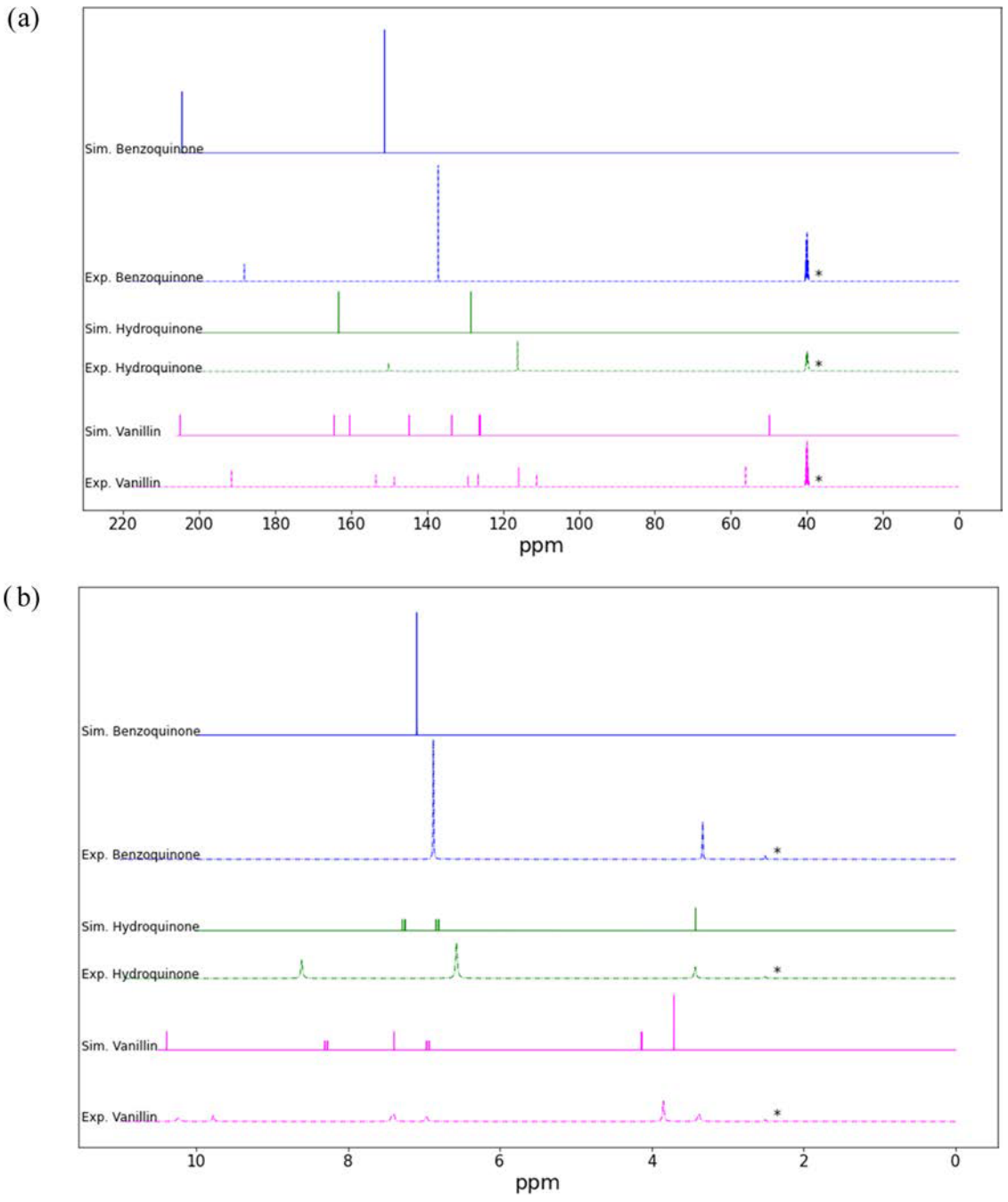

Figure 7. NMR spectra of model compounds (a) ^{13}C NMR and (b) ^{1}H NMR. * corresponds to the solvent peak.

CH_4), and OG10* ($S\beta O4S\beta 5G\beta O4G\text{-}H_2\text{-}CH_4$) with Gibbs free energies of 11.75, 13.12, and 12.35 kJ/mol, respectively. After balancing the structures, all tetramers can continue the demethylation reaction due to the greater number of OH and methyl groups available for their number of monomers. Figure 5 shows a detailed representation of the most stable tetramers through pathways 1 and 2.

In all of the oligomers, the most stable structures contain a greater number of $\beta 5$ bonds. This type of bond connecting the lignin units facilitates the stability of the molecule due to the conjugated C−C bonds. Tables S1−S3 show a detailed representation of all of the lignin oligomers. In addition, the coordinates corresponding to all optimized structures in their ground states can be found in the Supporting Information.

3.2. FTIR and NMR Spectra Calculations. *3.2.1. Model Compound Validation.* To validate the FTIR and NMR spectra obtained from electronic structure calculations, we decided to compare the calculated and experimental values of phenolic model compounds: vanillin, hydroquinone, and benzoquinone. To the best of our knowledge, samples of the oligomers listed in Figures 3−5 are not available in the literature. Figures 6 and 7 show the FTIR spectra fingerprint regions and the ^{13}C- and ^{1}H NMR of the model compounds' spectra, respectively. The model compounds are dotted lines, and the simulated spectra are solid lines. The spectra in the fingerprint region of the compounds are similar. The peaks that are clearly identified in the experimental spectrum can be observed in the simulated spectrum for vanillin, hydroquinone, and benzoquinone.

https://doi.org/10.1021/acs.energyfuels.2c04292
Energy Fuels 2023, 37, 5189−5205

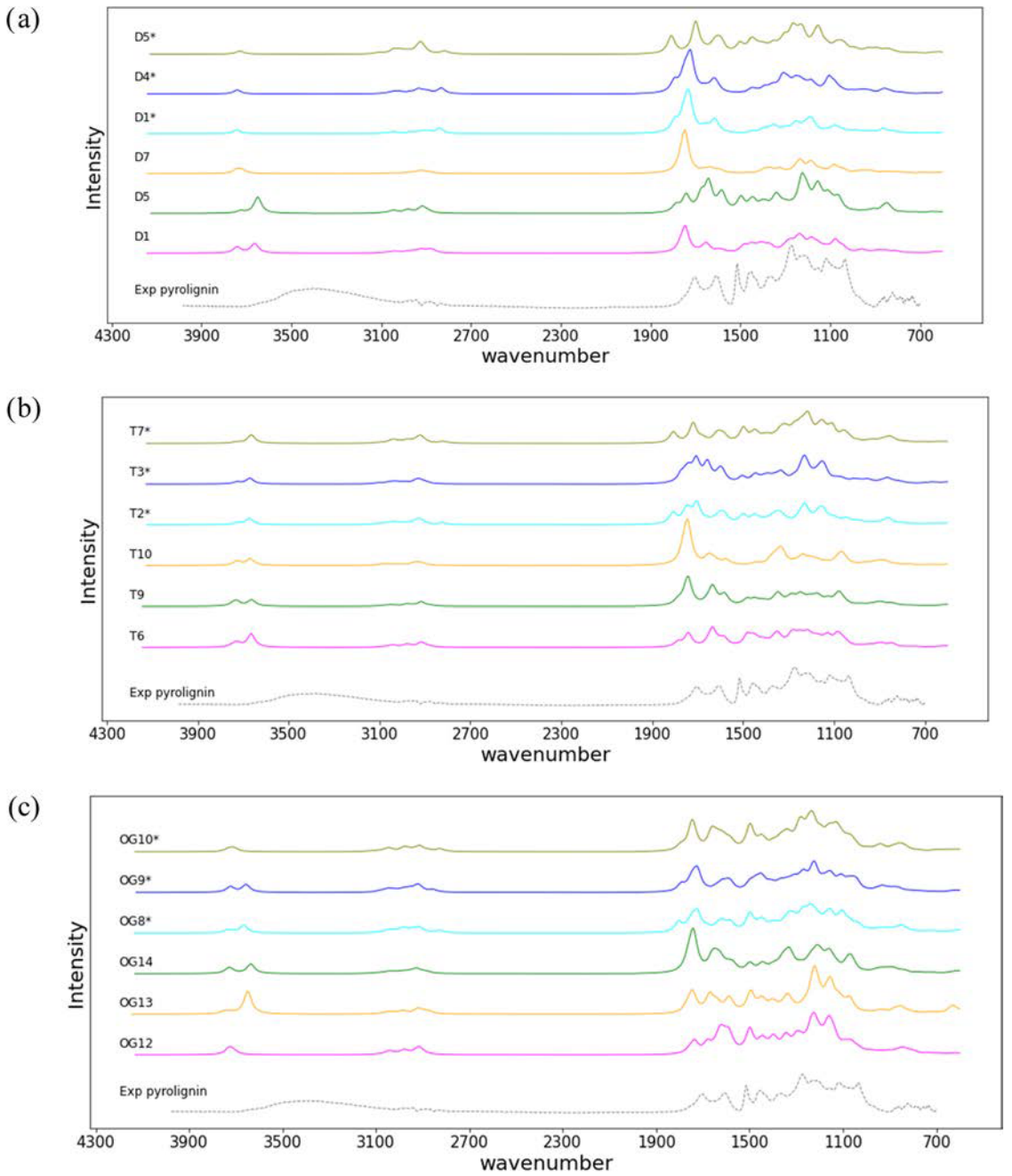

Figure 8. FTIR spectra of the proposed lignin oligomers: (a) dimers, (b) trimers, and (c) tetramers.

Additionally, the obtained spectra were compared to the FTIR spectra reported in the literature for these compounds, resulting in a spectrum similar to those found in previous studies.[51,52] The simulation parameters show good fitting of the model compounds and can be used to simulate these kinds of molecules. Although the peak locations present qualitative agreement, electronic structure calculations still lack accuracy due to the harmonic oscillator approximation. Figure 7 shows the ^{13}C- and ^{1}H NMR spectra of the model compounds to compare the experimental and simulated ones.

Bars of the simulated model compounds tend to be located to the right of the experimental peaks for carbon and hydrogen for vanillin, hydroquinone, and benzoquinone as model compounds. The peaks around 40 ppm for the experimental ^{13}C NMR and 2.3 ppm for the experimental ^{1}H NMR correspond to the solvent DMSO-d_6 used during the experiment. In addition, the simulated FTIR and NMR spectra were calculated in a gas-phase simulation, while the experimental FTIR and NMR spectra were obtained at a liquid phase. This also justifies the difference in the experimental and simulated FTIR and NMR peaks, even though the fitting between the simulated and experimental data is close enough to use the simulated FTIR and NMR spectra to characterize the proposed oligomer structures. Although peak locations present qualitative agreement, electronic structure calculations still lack accuracy due to the harmonic oscillator approximation. This does not capture anharmonic vibrational modes; therefore, it could disagree with experimental measurements. The adjustment value has not been extensively

https://doi.org/10.1021/acs.energyfuels.2c04292
Energy Fuels 2023, 37, 5189−5205

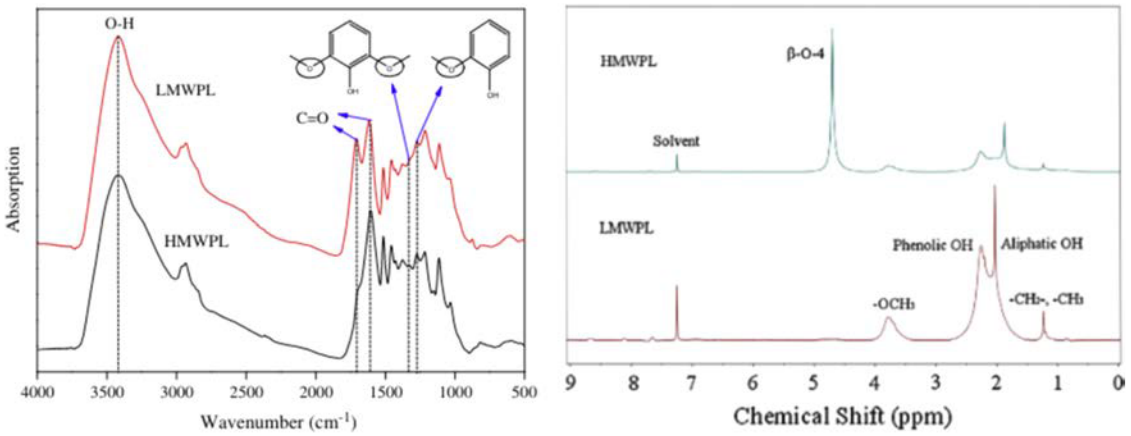

Figure 9. FTIR and ^{1}H NMR experimental spectra of low (red line) and high (black and blue line) molecular weight of pyrolytic lignin. Reprinted from ref 54 with permission from Elsevier.

discussed in the literature; then, a new value could allow a greater similarity between the spectra.

3.2.2. Information on Resulting Oligomers. The FTIR spectra of the 3 most probable simulated compounds for dimers, trimers, and tetramers are shown in Figure 8. The rest of the FTIR spectra of the proposed oligomers are presented in Figures S3−S7. These spectra can be compared with the experimental pyrolitic lignin based on the spectra of a water-insoluble fraction of biomass pyrolysis bio-oil that is reported in the literature. Figure 8 shows the FTIR spectra of lignin oligomers. The absorption peaks at 2971 and 2870 cm^{-1} correspond to methyl groups. In this band, the intensity is lower in the dimers and trimers that have undergone complete demethylation of the molecule since they have a limited amount of methyl groups, as would be expected for such compounds. In addition, the structure with more than one demethylation, like D7, T9, T10, OG13, and OG14, have lower intensity in these peaks. The shoulders in 1712 and 1673 cm^{-1} indicate unconjugated and conjugated carbonyl groups, respectively. The former can be attributed to unconjugated carbonyl from ester groups and the latter to conjugated aryl ketones. The peak at 1673 cm^{-1} is more intense for dimers because of the presence of conjugated carbonyl in its structure. This is the case of the trimer T10 and tetramer OG14, which present this intense peak because all of the carbonyl groups in its structure are conjugated.

Peaks around 1606−1336 cm^{-1} are related to aromatic skeletal vibration caused by C═O stretching, C−H deformations, asymmetry in $-CH_3$ and $-CH_2$, and the chemical groups that conform the lignin oligomers. The skeletal vibration of C−O present on syringyl units was identified at 1332 and 1116 cm^{-1}, while in the guaiacyl units, it is in the 1275 and 1154 cm^{-1} peaks, thus confirming the presence of S and G units in those oligomers because of the high thermal stability of methoxyl groups attached to aromatic rings.[44] Finally, the peaks at 1366, 1216, 1035, and 989 cm^{-1} could be related to the aliphatic side chains, carbonyls, and unsaturated double bonds, as has been suggested in other reports.[53] The experimental pyrolytic lignin spectrum report in Figure 8 was obtained using pyrolitic lignin powder through a multi-step solvent process with extraction cold-water precipitation and dichloromethane extraction of pyrolysis bio-oil.

The spectrum in Figure 8 is compared with the spectrum report by Wang et al.[54] in Figure 9 obtained by separating bio-oil using solvents to get high-molecular-weight and low-molecular-weight pyrolytic lignin. In contrast, peaks at 1700 cm^{-1} can be identified in the pyrolytic lignin. They are related to the vibration of the aromatic bonds caused by C═O at 1400 cm^{-1}, which may have to do with the deformations and asymmetries of the CH_3 and CH_2 chemical groups. These peaks were also identified in the benzoquinones reported in this study. However, in pyrolytic lignin, there is a peak at 3450 cm^{-1} related to the O−H bonds, which was not observed in the spectra of the benzoquinones reported in this study. According to the FTIR results, oligomers D5 (SβO4S-CH_4), T3* (Gβ5GβO4S-H_2-CH_4), and OG13 (GβO4SβO4Sβ5G-2CH_4) have a spectrum and therefore a more similar structure if compared with the experimental pyrolytic lignin used in this study. Another simulated information that we can use to analyze is NMR spectra. These spectra were used to define the interunit bonds of proposed oligomer structures. ^{1}H NMR simulated spectra of the pyrolitic lignin are presented in Figure 10.

Signals at 8.0−6.0 ppm can be attributed to aromatic and double-bond protons. In contrast, dimers only have two aromatic rings compared to trimers and tetramers; therefore, they have strong signals in that range. Additionally, signals between 4.1 and 3.6 ppm are related to methoxy groups found in these oligomers due to the presence of G and S units; the signal intensity is proportional to the number of monomers in the lignin oligomers; hence, it is possible to see more signals in tetramers than in dimers' spectra. Peaks between 3 and 0.5 ppm can be attributed to hydrogen in CH_2 and CH_3 groups; this signal is stronger as there are more monomers in the polymer chain. Also, in contrast with the different pathways, the most probable structures through pathway 2 have lower signals in this region because they balance using their own atoms and form quinones when reacting with CH_3 groups.

In the case of trimers and tetramers—since the structures can have a higher number of demethylations—the signal gets more intense because the methoxy bond is broken to produce methane and forms the quinone group. Peaks at 4.5−4.2, 9.3−8.1, and 1.5−0.5 ppm imply that the oligomers contain benzyl alcohol, phenolic, and aliphatic groups, respectively. The results indicate that pyrolitic lignin contains many unsaturated groups.[53]

On the other hand, the ^{1}H NMR simulated spectrum for pyrolitic lignin is similar to the one reported by Wang et al.[53]

https://doi.org/10.1021/acs.energyfuels.2c04292
Energy Fuels 2023, 37, 5189−5205

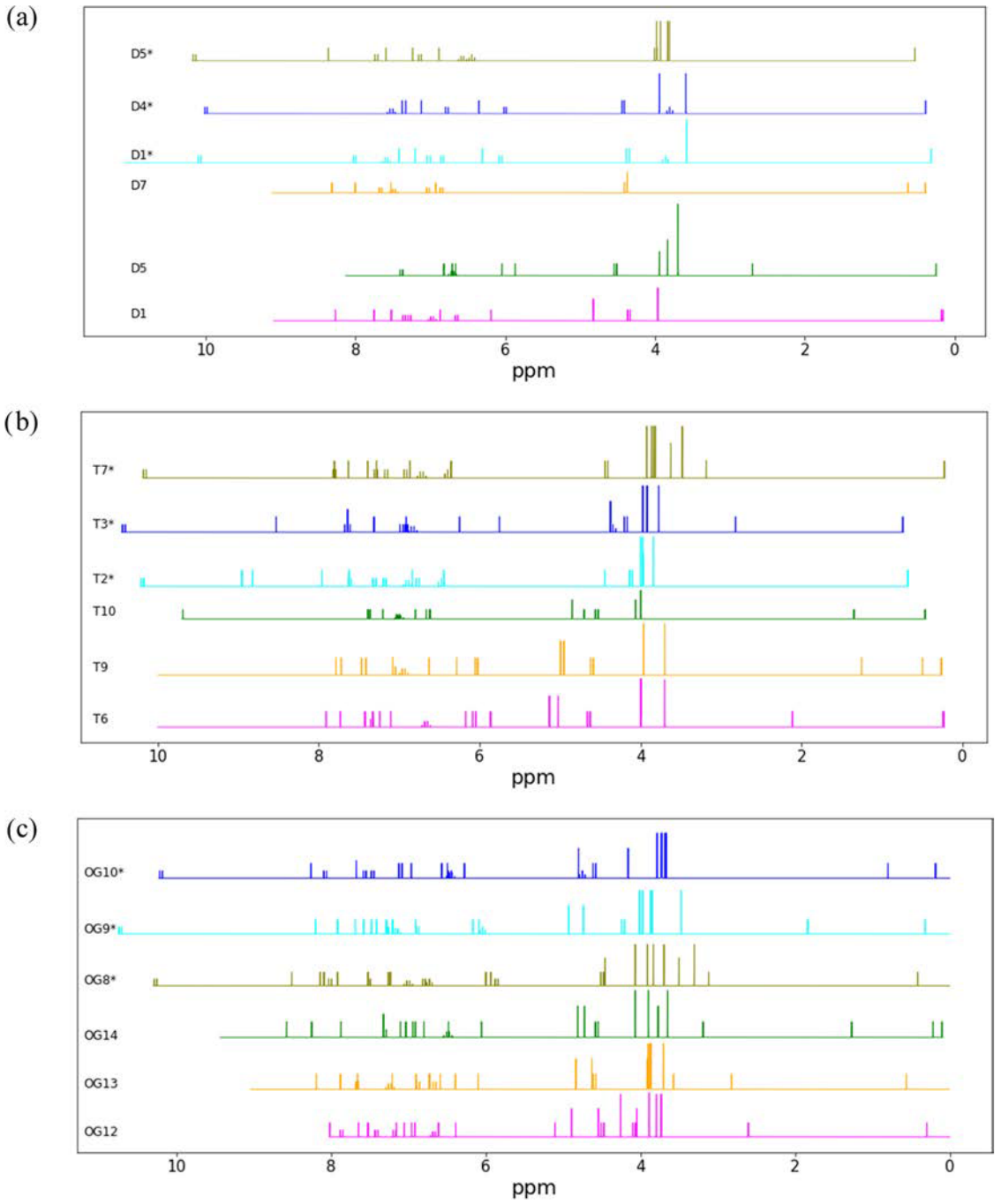

Figure 10. ^{1}H NMR simulated spectra of the proposed lignin oligomers: (a) dimers, (b) trimers, and (c) tetramers.

in Figure 9. The low-molecular-weight lignin is similar to dimers and trimers, and the high-molecular-weight pyrolitic lignin is similar to tetramer simulated spectra, especially in the peaks between 4 and 3.5 ppm related to hydrogen from methoxy groups. Tetramers have a longer polymer chain with G and S units if we compare the simulated spectra with the experimental one. In addition, lighter pyrolytic lignin has a more intense signal between 1 and 3 ppm, mainly related to the presence of aromatic and aliphatic OH groups because methyl groups are released to form methane. Benzoquinone molecules that could represent pyrolytic lignin bear a close resemblance to the spectrum of heavy pyrolytic lignin.

The interunit bonds in each oligomer were calculated from the ^{13}C NMR spectra, as shown in Figure 11. The aromatic region can be divided into oxygenated aromatic (166−142 ppm), condensed aromatic (142−125 ppm), and protonated aromatic (125−102 ppm) regions. In the first region, signals at 152 and 138 ppm originate from the $\beta O4$ structure in S-type carbon, which confirms the cleavage of the $\beta O4$ linkage by the pyrolysis process in the OG oligomers. Some of them have peaks in the condensed aromatic region. These structures still have methoxy groups that could form new quinones. Moreover, signals around 60 ppm are related to the propane side chain of carbon in the $\beta O4$ structure.[55] This confirms the propane side chain located in the OG oligomers. Signals from syringyl residues (C_2/C_6 at 108/104 ppm) are not present in this spectrum, supporting that quinones form mainly through demethylation of the syringyl initial structure. Additionally,

https://doi.org/10.1021/acs.energyfuels.2c04292
Energy Fuels 2023, 37, 5189−5205

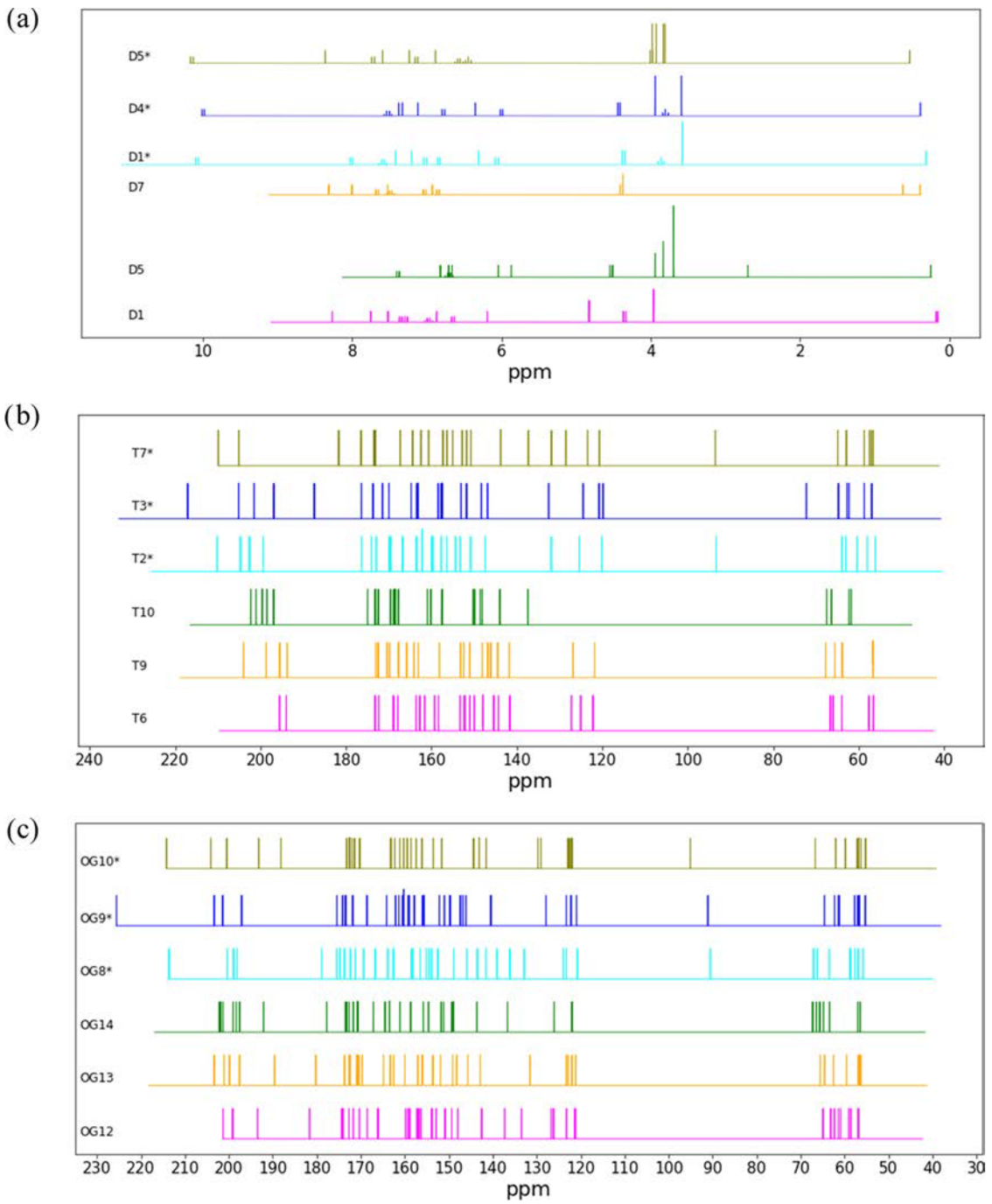

Figure 11. C NMR simulated spectra of the proposed lignin oligomers: (a) dimers, (b) trimers, and (c) tetramers.

even if this spectrum is only a trimer representation of the pyrolytic lignin, its shape is similar to the NMR spectra found in the literature for the water-insoluble fraction of the pyrolysis bio-oil or pyrolytic lignin.[56] The ^{13}C- and ^{1}H NMR spectra for all of the proposed oligomers are present in Figures S8–S17.

3.3. Thermophysical Properties. The thermophysical properties to be estimated are shown in Tables 5–7. The molecular structures of the demethylated lignin oligomers were analyzed and distributed into sets of structural groups in accordance with the functional groups proposed in the literature. These properties could be relevant to design new bio-oil upgrading systems such as distillers and condensers.

The calculated normal boiling points of the simulated oligomers were between 624 and 790 K for dimers, 720 and 908 K for trimers, and 800 and 1080 K for tetramers. These results resemble those reported in the literature, where the upper calculated values correspond to larger oligomers. Additionally, the calculated ranges of values for the trimers and tetramers are higher than the typical fast pyrolysis temperatures (773 K). This supports the hypothesis that heavy lignin oligomers (trimers or bigger) are ejected as aerosols during the pyrolysis reaction rather than vaporized.[58,59] Compared to the evaluated group additivity methods, the Yuan method presents lower values of the oligomers' normal boiling point, while the Satou et al. method presents the highest values, as shown in Tables 5–7. As the number of rings in the system increases, so does the normal boiling point. However, as the oligomers have a greater number of quinone

https://doi.org/10.1021/acs.energyfuels.2c04292
Energy Fuels 2023, 37, 5189–5205

Table 5. Estimated Thermophysical Properties of Proposed Lignin Dimers

physical property	symbol	author	D1	D5	D7	D1*	D4*	D5*
normal boiling point, K	T_b	Satou et al.[31]	748.6	790.0	736.1	747.1	769.0	798.6
		Yuan et al.[32]	636.4	658.3	624.6	636.4	647.6	668.4
		Stein and Brown[30]	713.7	782.1	552.5	632.3	754.7	676.6
critical temperature, K	T_c	Joback and Reid[57]	4715.9	4764.6	3754.9	4925.1	4885.7	5058.5
		Lydersen[33]	936.6	981.8	918.5	928.4	917.7	918.7
critical volume, m^3K/mol	V_c	Joback and Reid[57]	1116	1190	1115	1095	1233	1233
		Lydersen[33]	1325	1293	828.0	631.0	763.0	737.0
critical pressure, MPa	P_c	Lydersen[33]	19.7	15.9	21.8	19.2	14.2	19.8
Hansen solubility parameters, $MPa^{1/2}$	δ_d	Stefanis and Panayiotou[36]	22.1	21.1	25.1	24.8	20.9	24.9
	δ_h		19.9	21.3	25.7	25.5	21.7	27.2
	δ_{hb}		31.3	38.6	27.5	21.3	17.8	21.8
liquid heat capacity at 293.15 K, J/mol·K	$C_{p,l}$	Chueh and Swanson[37]	166.5	181.3	158.2	161.1	184.4	175.9
solid heat capacity at 293.15 K, J/mol·K	$C_{p,s}$	Hurst and Harrinson[38]	423.5	502.4	382.4	255	268.4	295.2
Gas heat capacity at constant pressure at 300 K, kJ/mol·K	$C_{p,g}$	Harrison and Seaton[39]	272.5	326.0	247.5	262.8	289.6	341.3
gas standard enthalpy of formation, KJ/mol	$\Delta H^\circ_{f,G}$	Joback[57]	−2791	−3478	−2367	−2731	−3265	−3030
gas standard Gibbs free energy, kJ/mol	$\Delta G^\circ_{f,G}$	Joback[57]	−1150	−1594	−757	−1278	−1455	−1270
gas heat capacity at constant volume, J/mol·K	C_v	DFT calculation	720.2	851.6	646.9	692.1	829.9	758.7
dipole moment, Debye	μ	DFT calculation	9.1	7.9	8.0	9.9	6.4	9.7

Table 6. Estimated Thermophysical Properties of the Proposed Lignin Trimers

physical property	symbol	author	T6	T9	T10	T2*	T3*	T7*
normal boiling point, K	T_b	Satou et al.[31]	908.6	900.8	893.1	907.6	907.67	915.3
		Yuan et al.[32]	736.2	728.8	721.1	736.2	736.2	743.3
		Stein and Brown[30]	949.9	881.2	795.3	894.4	881.5	973.2
critical temperature, K	T_c	Joback and Reid[57]	5084.5	5172.2	4783.4	5473.3	5508.4	5367.0
		Lydersen[33]	970.9	1110.5	1064.0	875.6	880.8	884.2
critical volume, m^3K/mol	V_c	Joback and Reid[57]	1666	1602	1499	1657	1689	1712
		Lydersen[33]	1054	1042	1292	1061	1087	1090
critical pressure, MPa	P_c	Lydersen[33]	10.6	11.9	13.7	11.2	11.4	10.2
Hansen solubility parameters, $MPa^{1/2}$	δ_d	Stefanis and Panayiotou[36]	22.8	25.6	29.6	27.9	26.0	22.6
	δ_h		29.8	32.4	37.9	36.4	33.7	29.7
	δ_{hb}		30.7	34.1	38.0	28.1	28.2	24.5
liquid heat capacity at 293.15 K, J/mol·K	$C_{p,l}$	Chueh and Swanson[37]	257.7	251.6	243.2	232.7	249.8	255.9
Solid heat capacity at 293.15 K, J/mol·K	$C_{p,s}$	Hurst and Harrinson[38]	687.7	646.6	605.4	402.6	402.6	416.0
gas heat capacity at constant pressure at 300 K, kJ/mol·K	$C_{p,g}$	Harrison and Seaton[39]	438.6	413.6	388.6	428.9	428.9	453.9
gas standard enthalpy of formation, KJ/mol	$\Delta H^\circ_{f,G}$	Joback[57]	−3650	−5095	−3247	−4682	−4488	−4343
gas standard Gibbs free energy, kJ/mol	$\Delta G^\circ_{f,G}$	Joback[57]	−1190	−2515	−662	−2132	−1906	−1686
gas heat capacity at constant volume,	C_v	DFT calculation	1179.4	1106.9	1033.9	1150.0	1151.2	1122.4
dipole moment, Debye	μ	DFT calculation	11.8	4.5	8.8	9.1	11.2	5.5

groups (those that undergo more than one demethylation), the boiling point values decrease. Although there are no reports of experimental values of this property, the theoretical values reported by Terrell et al.[14] for the boiling point depending on molecular weight coincide with the values presented in this work. On the contrary, the values reported in this work differ from those reported by Fonts et al.[18] for high and low molecular mass pyrolytic lignin, which are 3496 and 1637 K, respectively. This may be due to the fact that the Joback method—used by Fonts—is not adequate when large molecules such as lignin oligomers are involved. Stein and Brown[30] have shown previously that group contribution estimates for normal boiling point tend to diverge from experimental values around temperatures greater than 600 K. Therefore, this work used adjusted methods for this type of system.

Hansen solubility parameters are useful in valorization processes of bio-oil fractions because they are related to the intermolecular forces between compounds. Therefore, they are relevant in liquid−liquid extraction systems to select the solvent in analytical and industrial scale applications. The Hansen solubility parameter considers dispersion forces (δ_d), dipole−dipole forces (δ_{dh}), and hydrogen bonding (δ_h). The values reported in Tables 5−7 show behavior similar to that of the normal boiling point, as structures with more molecules (monomers) and quinones present higher solubility values. Ethyl acetate, dichloromethane, and acetone may be suitable to extract the pyrolytic lignin fraction in bio-oil. The values in Tables 5−7 are similar to those reported by Fonts; however, they are higher than those reported by Terrell.[19] Liquid and solid heat capacity are used in the design of bio-oil upgrading systems and are reported in the tables.

The enthalpy of formation is necessary to calculate the energy balance of the pyrolysis reaction and subsequent processes like distillation and hydrotreatment, while the Gibbs free energy of the compounds is useful to analyze the

https://doi.org/10.1021/acs.energyfuels.2c04292
Energy Fuels 2023, 37, 5189−5205

Table 7. Estimated Thermophysical Properties of Lignin Tetramers

physical property	symbol	author	OG12	OG13	OG14	OG8*	OG9*	OG10*
normal boiling point, K	T_b	Satou et al.[31]	1068.6	1056.7	1045.5	1051.7	1052.4	1053.1
		Yuan et al.[32]	804.4	799.1	793.5	804.4	804.4	804.4
		Stein and Brown[30]	1204.9	118.2	1040.9	1123.6	1132.9	1123.6
critical temperature, K	T_c	Joback and Reid[57]	5719.5	5625.4	5765.9	5090.5	6078.2	5990.5
		Lydersen[33]	1026.4	968.1	1009.8	906.3	924.8	906.3
critical volume, m^3K/mol	V_c	Joback and Reid[57]	2208.0	2091.0	2100.0	2228.5	2167.5	228.5
		Lydersen[33]	2748.0	1294.0	1394.0	1519.0	1548.0	1519.0
critical pressure, MPa	P_c	Lydersen[33]	8.2	9.8	8.7	7.6	7.9	7.6
Hansen solubility parameters, $MPa^{1/2}$	δ_d	Stefanis and Panayiotou[36]	23.8	26.1	28.9	26.5	27.6	25.9
	δ_h		34.9	39.2	42.6	40.4	39.4	39.0
	δ_{hb}		44.6	40.6	44.5	34.7	41.9	34.4
liquid heat capacity at 293.15 K, J/mol·K	$C_{p,l}$	Chueh and Swanson[37]	348.8	340.4	329.0	340.9	340.3	340.9
Solid heat capacity at 293.15 K, J/mol·K	$C_{p,s}$	Hurst and Harrinson[38]	951.9	910.8	869.6	936.8	936.8	936.8
gas heat capacity at constant pressure at 300 K, kJ/mol·K	$C_{p,g}$	Harrison and Seaton[39]	604.8	579.8	554.8	595.1	595.1	595.1
gas standard enthalpy of formation, KJ/mol	$\Delta H^{\circ}_{f,G}$	Joback[57]	−6888	−7250	−7200	−6819	−6822	−6819
gas standard Gibbs free energy, kJ/mol	$\Delta G^{\circ}_{f,G}$	Joback[57]	−3083	−3642	−3636	−3164	−3193	−3164
gas heat capacity at constant volume,	C_v	DFT calculation	391.7	357.2	357.2	1610.2	1611.2	1610.8
dipole moment, Debye	μ	DFT calculation	10.2	8.2	8.2	7.4	9.2	11.0

spontaneity of a reaction. The dimers' results for these properties are consistent with the values reported by Fonts[18] for low molecular mass. The values are −1447.9 and −750.9 kJ/mol for the gas standard enthalpy of formation and gas standard Gibbs free energy for low molecular mass. The dimer molecular mass is around 370 amu, a value close to 400 amu for the low molecular weight compounds that were used in the reference. On the contrary, the trimer and tetramer molecular masses are around 550 and 750 amu, far from the 1050 amu that the reference used as a surrogate bio-oil, thus indicating again that the Joback method is not adequate for the size of the lignin oligomers.

4. CONCLUSIONS

Based on the results of this study, the following insights are proposed. Structures for dimer, trimer, and tetramer oligomers are suggested based on the demethylation reaction, as it is assumed to be one of the primary reactions occurring after depolymerization. Initial assignments were proposed starting with direct $\beta O4$ homolysis to generate two free radical fragments that can be either dimers, trimers, or tetramers. These radical fragments can stabilize by taking hydrogen radicals that may be in solution during the formation of the intermediate liquid (pathway 1) before the thermal ejection. Another pathway (pathway 2) could occur when the radicals use intramolecular hydrogen, turning themselves into stable products. Electronic structure calculations on model pyrolysis reactions show several structures of dimers, trimers, and tetramers depending on the Gibbs free energies of the reaction. The most probable oligomers have a $\beta 5$ bond and are conjugated structures. These kinds of bonds reduce the stability of G and S units caused by the conjugated C−C double bond and imply the formation of quinone methides. In addition, quinones can be an intermediate compound or a final product in lignin thermal decomposition in the biomass pyrolysis process, as suggested elsewhere.[45,46] According to the FTIR results, oligomers D5 ($S\beta O4S\text{-}CH_4$), T3* ($G\beta 5G\beta O4S\text{-}H_2\text{-}CH_4$), and OG13 ($G\beta O4S\beta O4S\beta 5G\text{-}2CH_4$) have a comparable spectrum and therefore a more similar structure if compared with the experimental pyrolitic lignin used in this study. The molecular structures of the demethylated lignin oligomers were analyzed and distributed into sets of structural groups according to the functional groupings proposed in the literature. These properties could be relevant in the design of new bio-oil upgrading systems such as distillers and condensers. The normal boiling points for both trimers and tetramers are higher than 773 K. This supports the hypothesis that heavy lignin oligomers are not vaporized but ejected during the pyrolysis reaction.

■ ASSOCIATED CONTENT

Supporting Information

The Supporting Information is available free of charge at https://pubs.acs.org/doi/10.1021/acs.energyfuels.2c04292.

Oligomer proposed mechanism for trimers and tetramers; NMR and FTIR spectra; and properties for all of the evaluated structures and optimized geometries for the structures (PDF)

■ AUTHOR INFORMATION

Corresponding Author

Manuel García-Pérez − *Department of Biological Systems Engineering, Washington State University, Pullman, Washington 99163, United States;* orcid.org/0000-0002-9386-2632; Email: mgarcia-perez@wsu.edu

Authors

Raiza Manrique − *Facultad de Minas, Universidad Nacional de Colombia, Medellín 50034, Colombia*

Evan Terrell − *USDA-ARS Southern Regional Research Center, New Orleans, Louisiana 701245, United States;* orcid.org/0000-0002-1079-4110

Pavlo Kostetskyy − *Department of Chemical and Biological Engineering, Northwestern University, Evanston, Illinois 60208, United States;* orcid.org/0000-0003-2796-0362

Farid Chejne − *Facultad de Minas, Universidad Nacional de Colombia, Medellín 50034, Colombia;* orcid.org/0000-0003-0445-7609

https://doi.org/10.1021/acs.energyfuels.2c04292
Energy Fuels 2023, 37, 5189−5205

Mariefel Olarte − *Pacific Northwest National Laboratory, Richland, Washington 99352, United States;* orcid.org/0000-0003-2989-1110

Linda Broadbelt − *Department of Chemical and Biological Engineering, Northwestern University, Evanston, Illinois 60208, United States;* orcid.org/0000-0003-4253-592X

Complete contact information is available at: https://pubs.acs.org/10.1021/acs.energyfuels.2c04292

Notes

The authors declare no competing financial interest.

■ ACKNOWLEDGMENTS

Mrs. Manrique thanks the project "Strategy of transformation of the Colombian energy sector in the horizon 2030" funded by the call 788 of Minciencias Scientific Ecosystem, Contract number FP44842-210-2018. The authors gratefully acknowledge the financial contributions from the US National Science Foundation (CBET 1926412) and the U.S. Department of Energy (DE-EE0008505). This project was also funded by the USDA/NIFA through Hatch Project WNP00701. This work was partially supported by the U.S. Department of Agriculture, Agricultural Research Service. Mention of trade names or commercial products is solely for the purpose of providing specific information and does not imply recommendation or endorsement by USDA. USDA is an equal opportunity provider and employer. Finally, the authors thank the Alliance for Biomass and Sustainability Research−ABISURE, Hermes code 53024, for its support in the realization of this study.

■ REFERENCES

(1) Hu, B.; Zhang, Z. x.; Xie, W. l.; Liu, J.; Li, Y.; Zhang, W. m.; Fu, H.; Lu, Q. Advances on the Fast Pyrolysis of Biomass for the Selective Preparation of Phenolic Compounds. *Fuel Process. Technol.* **2022**, *237*, 107465.

(2) Wang, S.; Dai, G.; Yang, H.; Luo, Z. Lignocellulosic Biomass Pyrolysis Mechanism: A State-of-the-Art Review. *Prog. Energy Combust. Sci.* **2017**, *62*, 33−86.

(3) Mohan, D.; et al. Pyrolysis of Wood/Biomass for Bio-Oil: A Critical Review. *Energy Fuels* **2017**, *20*, 848−889.

(4) Zhang, L.; Zhang, S.; Hu, X.; Gholizadeh, M. Progress in Application of the Pyrolytic Lignin from Pyrolysis of Biomass. *Chem. Eng. J.* **2021**, *419*, 129560.

(5) Ponnusamy, V. K.; Nguyen, D. D.; Dharmaraja, J.; Shobana, S.; Banu, J. R.; Saratale, R. G.; Chang, S. W.; Kumar, G. A Review on Lignin Structure, Pretreatments, Fermentation Reactions and Biorefinery Potential. *Bioresour. Technol.* **2019**, *271*, 462−472.

(6) Ralph, J.; Lapierre, C.; Boerjan, W. Lignin Structure and Its Engineering. *Curr. Opin. Biotechnol.* **2019**, *56*, 240−249.

(7) Rosini, E.; Allegretti, C.; Melis, R.; Cerioli, L.; Conti, G.; Pollegioni, L.; D'Arrigo, P. Cascade Enzymatic Cleavage of the β-O-4 Linkage in a Lignin Model Compound. *Catal. Sci. Technol.* **2016**, *6*, 2195−2205.

(8) Hosoya, T.; Kawamoto, H.; Saka, S. Role of Methoxyl Group in Char Formation from Lignin-Related Compounds. *J. Anal. Appl. Pyrolysis* **2009**, *84*, 79−83.

(9) Jiang, X.; Lu, Q.; Hu, B.; Liu, J.; Dong, C.; Yang, Y. Intermolecular Interaction Mechanism of Lignin Pyrolysis: A Joint Theoretical and Experimental Study. *Fuel* **2018**, *215*, 386−394.

(10) Hu, B.; Xie, W. L.; Li, Y.; Zhang, Z. X.; Liu, J.; Zhang, B.; Wang, T. P.; Lu, Q. Hydroxyl-Assisted Hydrogen Transfer Interaction in Lignin Pyrolysis: An Extended Concerted Interaction Mechanism. *Energy Fuels* **2021**, *35*, 13170−13180.

(11) Huang, Y.; Wang, H.; Zhang, X.; Zhang, Q.; Wang, C.; Ma, L. CO2 Pyrolysis Kinetics and Characteristics of Lignin-Rich Hydrolysis Residue Produced from a Tandem Process of Steam-Stripping and Acid Hydrolysis. *Fuel* **2022**, *316*, 123361.

(12) Wang, L.; Fang, Y.; Yin, J.; Li, X.; Jiang, J.; Zhang, Y.; Yang, H. Fast Pyrolysis of Guaiacyl-Syringyl (GS) Type Milled Wood Lignin: Product Characteristics and CH4 Formation Mechanism Study. *Sci. Total Environ.* **2022**, *838*, 156395.

(13) Huang, J.; Liu, C.; Wu, D.; Tong, H.; Ren, L. Density Functional Theory Studies on Pyrolysis Mechanism of β-O-4 Type Lignin Dimer Model Compound. *J. Anal. Appl. Pyrolysis* **2014**, *109*, 98−108.

(14) Terrell, E.; Garcia-Perez, M. Vacuum Pyrolysis of Hybrid Poplar Milled Wood Lignin with Fourier Transform-Ion Cyclotron Resonance Mass Spectrometry Analysis of Feedstock and Products for the Elucidation of Reaction Mechanisms. *Energy Fuels* **2020**, *34*, 14249−14263.

(15) Fu, X.; Li, Q.; Hu, C. Identification and Structural Characterization of Oligomers Formed from the Pyrolysis of Biomass. *J. Anal. Appl. Pyrolysis* **2019**, *144*, 104696.

(16) Dhyani, V.; Bhaskar, T. A Comprehensive Review on the Pyrolysis of Lignocellulosic Biomass. *Renewable Energy* **2018**, *129*, 695−716.

(17) Huang, J.; Liu, C.; Tong, H.; Li, W.; Wu, D. A Density Functional Theory Study on Formation Mechanism of CO, CO2 and CH4 in Pyrolysis of Lignin. *Comput. Theor. Chem.* **2014**, *1045*, 1−9.

(18) Fonts, I.; Atienza-Martínez, M.; Carstensen, H. H.; Benés, M.; Pires, A. P. P.; Garcia-Perez, M.; Bilbao, R. Thermodynamic and Physical Property Estimation of Compounds Derived from the Fast Pyrolysis of Lignocellulosic Materials. *Energy Fuels* **2021**, *35*, 17114−17137.

(19) Terrell, E. Estimation of Hansen Solubility Parameters with Regularized Regression for Biomass Conversion Products: An Application of Adaptable Group Contribution. *Chem. Eng. Sci.* **2022**, *248*, 117184.

(20) Kawamoto, H. Lignin Pyrolysis Reactions. *J. Wood Sci.* **2017**, *63*, 117−132.

(21) Leng, E.; Guo, Y.; Chen, J.; Liu, S.; E, J.; Xue, Y. A Comprehensive Review on Lignin Pyrolysis: Mechanism, Modeling and the Effects of Inherent Metals in Biomass. *Fuel* **2022**, *309*, No. 122102.

(22) Britt, P. F.; Buchanan, A. C.; Cooney, M. J.; Martineau, D. R. Flash Vacuum Pyrolysis of Methoxy-Substituted Lignin Model Compounds. *J. Org. Chem.* **2000**, *65*, 1376−1389.

(23) Britt, P. F.; Buchanan, A. C.; Malcolm, E. A. Thermolysis of Phenethyl Phenyl Ether: A Model for Ether Linkages in Lignin and Low Rank Coal. *J. Org. Chem.* **1995**, *60*, 6523−6536.

(24) Zhou, S.; Pecha, B.; van Kuppevelt, M.; McDonald, A. G.; Garcia-Perez, M. Slow and Fast Pyrolysis of Douglas-Fir Lignin: Importance of Liquid-Intermediate Formation on the Distribution of Products. *Biomass Bioenergy* **2014**, *66*, 398−409.

(25) Fan, Y.; Lei, M.; Han, Y.; Zhang, Z.; Kong, X.; Xu, W.; Li, M.; Zhang, H.; Xiao, R.; Liu, C. Elucidating Radical-Mediated Pyrolysis Behaviors of Preoxidized Lignins. *Bioresour. Technol.* **2022**, *350*, 126908.

(26) Lei, M.; Wu, S.; Liang, J.; Liu, C. Comprehensive Understanding the Chemical Structure Evolution and Crucial Intermediate Radical in Situ Observation in Enzymatic Hydrolysis/Mild Acidolysis Lignin Pyrolysis. *J. Anal. Appl. Pyrolysis* **2019**, *138*, 249−260.

(27) Younker, J. M.; Beste, A.; Buchanan, A. C. Computational Study of Bond Dissociation Enthalpies for Substituted β-O-4 Lignin Model Compounds. *ChemPhysChem* **2011**, *12*, 3556−3565.

(28) Ünal, Y.; Nassif, W.; Özaydin, B. C.; Sayin, K. Scale Factor Database for the Vibration Frequencies Calculated in M06-2X, One of the DFT Methods. *Vib. Spectrosc.* **2021**, *112*, 103189.

(29) Stankovikj, F.; Garcia-perez, M. TG-FTIR Method for the Characterization of Bio-Oils in Chemical Families. *Energy Fuels* **2017**, *31*, 1689−1701.

(30) Stein, S. E.; Brown, R. L. Estimation of Normal Boiling Points from Group Contributions. *J. Chem. Inf. Model.* **1994**, *34*, 581−587.

(31) Satou, M.; Itoh, D.; Hattori, H.; Yoshida, T. Evaluation of Ring Size Distribution in a Heavy Oil Based on Boiling Point and Molecular Weight Distributions. *Fuel* **2000**, *79*, 339−348.
(32) Yuan, W.; Hansen, A. C.; Zhang, Q. Vapor Pressure and Normal Boiling Point Predictions for Pure Methyl Esters and Biodiesel Fuels. *Fuel* **2005**, *84*, 943−950.
(33) Lydersen, Al. L.; Greenkorn, R. A.; Hougen, O. A. *Estimation of Critical Properties of Organic Compounds*; Madison, 1955. https://scholar.google.com/scholar_lookup?hl=en&publication_year=1955&author=A.+L.+Lydersen&author=R.+A.+Greenkorn&author=O.+A.+Hougen&title=Estimation+of+Critical+Properties+of+Organic+Compounds (accessed 2023-02-06).
(34) Joback, K. G. A Unified Approach to Physical Property Estimation Using Multivariate Statistical Techniques, Massachusetts Institute of Technology, 1984, https://dspace.mit.edu/handle/1721.1/15374.
(35) Joback, K. G.; Reid, R. C. Estimation of Pure-Component Properties from Group-Contributions. *Chem. Eng. Commun.* **1987**, *57*, 233−243.
(36) Stefanis, E.; Panayiotou, C. Prediction of Hansen Solubility Parameters with a New Group-Contribution Method. *Int. J. Thermophys.* **2008**, *29*, 568−585.
(37) Chueh, C. F.; Swanson, A. C. Estimation of Liquid Heat Capacity. *Can. J. Chem. Eng.* **1973**, *51*, 596−600.
(38) Hurst, J. E.; Harrison, B. K. Estimation of Liquid and Solid Heat Capacities Using a Modified Kopp's Rule. *Chem. Eng. Commun.* **1992**, *112*, 21−30.
(39) Harrison, B. K.; Seaton, W. H. Solution to Missing Group Problem for Estimation of Ideal Gas Heat Capacities. *Ind. Eng. Chem. Res.* **1988**, *27*, 1536−1540.
(40) Fonts, I.; Atienza-Martínez, M.; Carstensen, H. H.; Benés, M.; Pinheiro Pires, A. P.; Garcia-Perez, M.; Bilbao, R. Thermodynamic and Physical Property Estimation of Compounds Derived from the Fast Pyrolysis of Lignocellulosic Materials. *Energy Fuels* **2021**, *35*, 17114−17137.
(41) Lei, M.; Wu, S.; Liu, C.; Liang, J.; Xiao, R. Revealing the Pyrolysis Behavior of 5-5′ Biphenyl-Type Lignin Fragment. Part I: A Mechanistic Study on Fragmentation via Experiments and Theoretical Calculation. *Fuel Process. Technol.* **2021**, *217*, 106812.
(42) Chen, D.; Cen, K.; Cao, X.; Chen, F.; Zhang, J.; Zhou, J. Insight into a New Phenolic-Leaching Pretreatment on Bamboo Pyrolysis: Release Characteristics of Pyrolytic Volatiles, Upgradation of Three Phase Products, Migration of Elements, and Energy Yield. *Renewable Sustainable Energy Rev.* **2021**, *136*, 110444.
(43) Li, C.; Gao, Y.; He, S.; Chi, H. Y.; Li, Z. C.; Zhou, X. X.; Yan, B. Quantification of Nanoplastic Uptake in Cucumber Plants by Pyrolysis Gas Chromatography/Mass Spectrometry. *Environ. Sci. Technol. Lett.* **2021**, *8*, 633−638.
(44) Asmadi, M.; Kawamoto, H.; Saka, S. Thermal Reactions of Guaiacol and Syringol as Lignin Model Aromatic Nuclei. *J. Anal. Appl. Pyrolysis* **2011**, *92*, 88−98.
(45) Pan, Z.; Puente-Urbina, A.; Bodi, A.; van Bokhoven, J. A.; Hemberger, P. Isomer-Dependent Catalytic Pyrolysis Mechanism of the Lignin Model Compounds Catechol, Resorcinol and Hydroquinone. *Chem. Sci.* **2021**, *12*, 3161−3169.
(46) Zhou, Q.; Luo, Z.; Li, G.; Li, S. EPR Detection of Key Radicals during Coking Process of Lignin Monomer Pyrolysis. *J. Anal. Appl. Pyrolysis* **2020**, *152*, 104948.
(47) Hosoya, T.; Kawamoto, H.; Saka, S. Role of Methoxyl Group in Char Formation from Lignin-Related Compounds. *J. Anal. Appl. Pyrolysis* **2009**, *84*, 79−83.
(48) Paul, G. C.; Gajewski, J. Benzoquinone Methide: An Intermediate in the Gas-Phase Pyrolysis of Chroman. *J. Org. Chem.* **1993**, *58*, 5060−5062.
(49) Kotake, T.; Kawamoto, H.; Saka, S. Pyrolytic Formation of Monomers from Hardwood Lignin as Studied from the Reactivities of the Primary Products. *J. Anal. Appl. Pyrolysis* **2015**, *113*, 57−64.
(50) Terrel, E.; Garcia-Perez, M. Novel Strategy to Analyze FT-ICR MS Data of Biomass Pyrolysis Oil for Oligomeric Structure Assignment. *Energy Fuels* **2020**, *34*, 8466−8481.
(51) Aktaş, N.; Şahiner, N.; Kantoğlu, Ö.; Salih, B.; Tanyolaç, A. Biosynthesis and Characterization of Laccase Catalyzed Poly-(Catechol). *J. Polym. Environ.* **2003**, *11*, 123−128.
(52) Hsieh, P. W.; Al-Suwayeh, S. A.; Fang, C. L.; Lin, C. F.; Chen, C. C.; Fang, J. Y. The Co-Drug of Conjugated Hydroquinone and Azelaic Acid to Enhance Topical Skin Targeting and Decrease Penetration through the Skin. *Eur. J. Pharm. Biopharm.* **2012**, *81*, 369−378.
(53) Wang, Y.; Wang, S.; Leng, F.; Chen, J.; Zhu, L.; Luo, Z. Separation and Characterization of Pyrolytic Lignins from the Heavy Fraction of Bio-Oil by Molecular Distillation. *Sep. Purif. Technol.* **2015**, *152*, 123−132.
(54) Wang, S.; Wang, Y.; Cai, Q.; Wang, X.; Jin, H.; Luo, Z. Multi-Step Separation of Monophenols and Pyrolytic Lignins from the Water-Insoluble Phase of Bio-Oil. *Sep. Purif. Technol.* **2014**, *122*, 248−255.
(55) Kim, J. Y.; Hwang, H.; Oh, S.; Kim, Y. S.; Kim, U. J.; Choi, J. W. Investigation of Structural Modification and Thermal Characteristics of Lignin after Heat Treatment. *Int. J. Biol. Macromol.* **2014**, *66*, 57−65.
(56) Scholze, B.; Hanser, C.; Meier, D. Characterization of the Water-Insoluble Fraction from Fast Pyrolysis Liquids (Pyrolytic Lignin) Part II. GPC, Carbonyl Goups, and 13 C-NMR. **2001**, *58*, 387 400. DOI: 10.1016/s0165-2370(00)00173-x.
(57) Joback, K. G. A Unified Approach to Physical Property Estimation Using Multivariate Statistical Techniques. Dissertation. Massachusetts Institute of Technology, 1984.
(58) Teixeira, A. R.; Mooney, K. G.; Kruger, J. S.; Williams, C. L.; Suszynski, W. J.; Schmidt, L. D.; Schmidt, D. P.; Dauenhauer, P. J. Aerosol Generation by Reactive Boiling Ejection of Molten Cellulose. *Energy Environ. Sci.* **2011**, *4*, 4306−4321.
(59) Pecha, M. B.; Terrell, E.; Montoya, J. I.; Stankovikj, F.; Broadbelt, L. J.; Chejne, F.; Garcia-Perez, M. Effect of Pressure on Pyrolysis of Milled Wood Lignin and Acid-Washed Hybrid Poplar Wood. *Ind. Eng. Chem. Res.* **2017**, *56*, 9079−9089.

https://doi.org/10.1021/acs.energyfuels.2c04292
Energy Fuels 2023, 37, 5189−5205